
Learning low-dimensional state embeddings and metastable clusters from time series data

Yifan Sun

Carnegie Mellon University
yifans@andrew.cmu.edu

Yaqi Duan

Princeton University
yaqid@princeton.edu

Hao Gong

Princeton University
hgong@princeton.edu

Mengdi Wang

Princeton University
mengdiw@princeton.edu

Abstract

This paper studies how to find compact state embeddings from high-dimensional Markov state trajectories, where the transition kernel has a small intrinsic rank. In the spirit of diffusion map, we propose an efficient method for learning a low-dimensional state embedding and capturing the process’s dynamics. This idea also leads to a kernel reshaping method for more accurate nonparametric estimation of the transition function. State embedding can be used to cluster states into metastable sets, thereby identifying the slow dynamics. Sharp statistical error bounds and misclassification rate are proved. Experiment on a simulated dynamical system shows that the state clustering method indeed reveals metastable structures. We also experiment with time series generated by layers of a Deep-Q-Network when playing an Atari game. The embedding method identifies game states to be similar if they share similar future events, even though their raw data are far different.

1 Introduction

High-dimensional time series is ubiquitous in scientific studies and machine learning. Finding compact representation from state-transition trajectories is often a prerequisite for uncovering the underlying physics and making accurate predictions. Suppose that we are given a Markov process $\{X_t\}$ taking values in $\Omega \subset \mathbb{R}^d$. Let $p(y|x)$ be the one-step transition density function (transition kernel) of the Markov process. In practice, state-transition trajectories may appear high-dimensional, but they are often generated by a system with fewer internal parameters and small intrinsic dimension.

In this paper, we focus on problems where the transition kernel $p(y|x)$ admits a low-rank decomposition structure. Low-rank or nearly low-rank nature of the transition kernel has been widely identified in scientific and engineering applications, e.g. molecular dynamics [RZMC11, SS13], periodized diffusion process [Går54], traffic transition data [ZW18, DKW19], Markov decision process and reinforcement learning [KAL16]. For reversible dynamical systems, leading eigenfunctions of p are related to metastable sets and slow dynamics [SS13]. Low-rank latent structures also helps state representation learning and dimension reduction in robotics and control [BSB⁺15].

Our goal is to estimate the transition kernel $p(\cdot|\cdot)$ from finite time series and find state representation in lower dimensions. For nonparametric estimation of probability distributions, one natural approach is the kernel mean embedding (KME). Our approach starts with a kernel space, but we “open up” the kernel function into a set of features. We will leverage the low-rankness of p in the spirit of diffusion map for dimension reduction. By using samples of transition pairs $\{(X_t, X_{t+1})\}$, we can estimate the “projection” of p onto the product feature space and finds its leading singular functions. This allows

us to learn state embeddings that preserve information about the transition dynamics. Our approach can be thought of as a generalization of diffusion map to nonreversible processes and Hilbert space. We show that, when the features can fully express the true p , the estimated state embeddings preserve the diffusion distances and can be further used to cluster states that share similar future paths, thereby finding metastable sets and long-term dynamics of the process.

The contributions of this paper are:

1. *KME Reshaping for more accurate estimation of p .* The method of KME reshaping is proposed to estimate p from dependent time series data. The method takes advantage of the low-rank structure of p and can be implemented efficiently in compact space. Theorem 1 gives a finite-sample error bound and shows that KME reshaping achieves significantly smaller error than plain KME.
2. *State embedding learning with statistical distortion guarantee.* In light of the diffusion map, we study state embedding by estimating the leading spectrum of the transition kernel. Theorems 2,3 show that the state embedding largely preserves the diffusion distance.
3. *State clustering with misclassification error bound.* Based on the state embeddings, we can further aggregate states to preserve the transition dynamics and find metastable sets. Theorem 4 establishes the statistical misclassification guarantee for continuous-state Markov processes.
4. *Experiments with diffusion process and Atari game.* The first experiment studies a simulated stochastic diffusion process, where the results validate the theoretical bounds and reveals metastable structures of the process. The second experiment studies the time series generated by a deep Q-network (DQN) trained on an Atari game. The raw time series is read from the last hidden layer as the DQN is run. The state embedding results demonstrate distinctive and interpretable clusters of game states. Remarkably, we observe that game states that are close in the embedding space share similar future moves, even if their raw data are far different.

To our best knowledge, our theoretical results on estimating p and state embedding are the first of their kind for continuous-state nonreversible Markov time series. Our methods and analyses leverage spectral properties of the transition kernel. We also provide the first statistical guarantee for partitioning the continuous state space according to diffusion distance.

Related Work Spectral dimension reduction methods find wide use in data analysis and scientific computing. Diffusion map is a prominent dimension reduction tool which applies to data analysis, graph partitioning and dynamical systems [LL06],[CKL⁺08]. For molecular dynamics, [SNL⁺11] showed that leading spectrum of transition operator contains information on slow dynamics of the system, and it can be used to identify coresets upon which a coarse-grained Markov state model could be built. [KSM18] extended the transfer operator theory to reproducing kernel spaces and pointed out the these operators are related to conditional mean embeddings of the transition distributions. See [KKS16, KNK⁺18] for surveys on data-driven dimension reduction methods for dynamical systems. They did not study statistical properties of these methods which motivated our research.

Nonparametric estimation of the Markov transition operator has been thoroughly studied, see [Yak79, Lac07, Sar14]. Among nonparametric methods, kernel mean embeddings are prominent for representing probability distributions [BTA04, SGSS07]. [SHSF09] extended kernel embedding methods to conditional distributions. [GLB⁺12] proposed to use conditional mean embedding to model Markov decision processes. See [MFSS17] for a survey on kernel mean embedding. None of these works considered low-rank estimation of Markov transition kernel, to our best knowledge.

Estimation of low-rank transition kernel was first considered by [ZW18] in the special case of finite-state Markov chains. [ZW18] used a singular thresholding method to estimate the transition matrix and proves near-optimal error upper and lower bounds. They also proved misclassification rate for state clustering when the chain is lumpable or aggregable. [LWZ18] studied a rank-constrained maximum likelihood estimator of the transition matrix. [DKW19] proposed a novel approach for finding state aggregation by spectral decomposing transition matrix and transforming singular vectors. For continuous-state reversible Markov chains, [LP18] studied the nonparametric estimation of transition kernel via Galerkin projection with spectral thresholding. They proved recovery error bounds when eigenvalues decay exponentially.

Notations For a function $f : \Omega \rightarrow \mathbb{R}$, we define $\|f\|_{L^2}^2 := \int_{\Omega} f(x)^2 dx$ and $\|f\|_{L^2(\pi)}^2 := \int_{\Omega} \pi(x) f(x)^2 dx$, respectively. For $g(\cdot, \cdot) \rightarrow \mathbb{R}$, we define $\|g(\cdot, \cdot)\|_{L^2(\pi) \times L^2} := (\int \pi(x) g(x, y)^2 dy dx)^{1/2}$. We use $\|\cdot\|$ to

denote the Euclidean norm of a vector. We let t_{mix} denote the mixing time of the Markov process [LP17], i.e., $t_{mix} = \min \{t \mid \text{TV}(P^t(\cdot \mid x), \pi(\cdot)) \leq \frac{1}{4}, \forall x \in \Omega\}$, where TV is the total variation divergence between two distributions. Let $\pi(x)$ be the density function of invariant measure of the Markov chain. Let $p(x, y)$ be the density of the invariant measure of the bivariate chain $\{(X_t, X_{t+1})\}_{t=0}^\infty$, i.e. $p(X_t, X_{t+1}) = \pi(X_t)p(X_{t+1} \mid X_t)$. We use $\mathbb{P}(\cdot)$ to denote probability of an event.

2 KME Reshaping for Estimating p

In this section we study the estimation of transition function p from a finite trajectory $\{X_t\}_{t=1}^n \subset \mathbb{R}^d$. We make following low-rank assumption regarding the transition kernel p , which is key to more accurate estimation.

Assumption 1. *There exist real-valued functions $\{u_k\}_{k=1}^r, \{v_k\}_{k=1}^r$ on Ω such that $p(y \mid x) := \sum_{k=1}^r \sigma_k u_k(x) v_k(y)$, where r is the rank.*

Due to the asymmetry of $p(\cdot, \cdot)$ and lack of reversibility, we use two reproducing kernel Hilbert spaces \mathcal{H} and $\tilde{\mathcal{H}}$ to embed the left and right side of p . Let K and \tilde{K} be the kernel functions for \mathcal{H} and $\tilde{\mathcal{H}}$ respectively. The Kernel Mean Embedding (KME) $\mu_p(x, y)$ of the joint distribution $p(x, y)$ into the product space $\mathcal{H} \times \tilde{\mathcal{H}}$ is defined by

$$\mu_p(x, y) := \int K(x, u) \tilde{K}(y, v) p(u, v) du dv.$$

Given sample transition pairs $\{(X_i, X'_i)\}_{i=1}^n$, the natural empirical KME estimator is $\tilde{\mu}_p(x, y) = \frac{1}{n} \sum_{i=1}^n K(X_i, x) \tilde{K}(X'_i, y)$. If data pairs are independent, one can show that the embedding error $\|\mu_p - \tilde{\mu}_p\|_{\mathcal{H} \times \tilde{\mathcal{H}}}$ is approximately $\sqrt{\frac{\mathbb{E}_{(X, Y) \sim p}[K(X, X) \tilde{K}(Y, Y)]}{n}}$ (Lemma 1 in Appendix). Next we propose a sharper KME estimator.

Suppose that the kernel functions K and \tilde{K} are continuous and symmetric semi-definite. Let $\{\Phi_j(x)\}_{j \in J}$ and $\{\tilde{\Phi}_j(x)\}_{j \in J}$ be the real-valued feature functions on Ω such that $K(x, y) = \sum_{j \in J} \Phi_j(x) \Phi_j(y)$, and $\tilde{K}(x, y) = \sum_{j \in J} \tilde{\Phi}_j(x) \tilde{\Phi}_j(y)$. In practice, if one is given a shift-invariant symmetric kernel function, we can generate finitely many random Fourier features to approximate the kernel [RR08]. In what follows we assume without loss of generality that J is finite of size N .

Let $\Phi(x) = [\Phi_1(x), \dots, \Phi_N(x)]^T \in \mathbb{R}^N$. We define the “projection” of p onto the feature space by

$$\mathbf{P} = \int p(x, y) \Phi(x) \tilde{\Phi}(y)^T dx dy. \quad (1)$$

Assumption 1 suggests that $\text{rank}(\mathbf{P}) \leq r$ (Lemma 2 in Appendix). Note that the KME of $p(x, y)$ is equivalent to $\mu_p(x, y) = \Phi(x)^T \mathbf{P} \tilde{\Phi}(y)$ (Lemma 3 in Appendix). The matrix \mathbf{P} is of finite dimensions, therefore we can estimate it tractably from the trajectory $\{X_t\}$ by

$$\hat{\mathbf{P}} := \frac{1}{n} \sum_{t=1}^n \Phi(X_t) \tilde{\Phi}(X_{t+1})^T. \quad (2)$$

Since the unknown \mathbf{P} is low-rank, we propose to apply singular value truncation to $\hat{\mathbf{P}}$ for obtaining a better KME estimator. The algorithm is given below:

Algorithm 1: Reshaping the Kernel Mean Embedding.

Input: $\{X_1, \dots, X_n\}, r$;

Get $\hat{\mathbf{P}}$ by (2), compute its SVD: $\hat{\mathbf{P}} = \hat{\mathbf{U}} \hat{\mathbf{\Sigma}} \hat{\mathbf{V}}^T$;

Let $\tilde{\mathbf{P}} := \hat{\mathbf{U}} \hat{\mathbf{\Sigma}}_{[1:r]} \hat{\mathbf{V}}^T$ be the best rank r approximation of $\hat{\mathbf{P}}$;

Let $\hat{\mu}_p(x, y) := \Phi(x)^T \tilde{\mathbf{P}} \tilde{\Phi}(y)$;

Output: $\hat{\mu}_p(x, y)$

We analyze the convergence rate of $\hat{\mu}_p$ to μ_p . Let $K_{max} := \max\{\sup_{x \in \Omega} K(x, x), \sup_{x \in \Omega} \tilde{K}(x, x)\}$. We define following kernel covariance matrices:

$$\mathbf{V}_1 = \mathbb{E}_{(X, Y) \sim p}[\Phi(X) \Phi(X)^T \tilde{K}(Y, Y)], \quad \mathbf{V}_2 = \mathbb{E}_{(X, Y) \sim p}[K(X, X) \tilde{\Phi}(Y) \tilde{\Phi}(Y)^T].$$

Let $\bar{\lambda} := \max\{\lambda_{\max}(\mathbf{V}_1), \lambda_{\max}(\mathbf{V}_2)\}$. We show the following finite-sample error bound.

Theorem 1 (KME Reshaping). *Let Assumption 1 hold. For any $\delta \in (0, 1)$, we have*

$$\|\mu_p - \hat{\mu}_p\|_{\mathcal{H} \times \tilde{\mathcal{H}}} = \|\mathbf{P} - \tilde{\mathbf{P}}\|_F \leq C\sqrt{r} \left(\sqrt{\frac{t_{\text{mix}} \bar{\lambda} \log(2t_{\text{mix}} N / \delta)}{n}} + \frac{t_{\text{mix}} K_{\max} \log(2t_{\text{mix}} N / \delta)}{3n} \right)$$

with probability at least $1 - \delta$, where C is a universal constant.

The KME reshaping method and Theorem 1 enjoys the following advantages:

1. **Improved accuracy compared to plain KME.** The plain KME $\tilde{\mu}_p$'s estimation error is approximately $\sqrt{\frac{\mathbb{E}_{(X,Y) \sim p}[K(X,X)\tilde{K}(Y,Y)]}{n}}$ (Appendix Lemma 1). Note that $\text{Tr}(\mathbf{V}_1) = \text{Tr}(\mathbf{V}_2) = \mathbb{E}_{(X,Y) \sim p}[K(X,X)\tilde{K}(Y,Y)]$. When $r \ll N$, we typically have $r\bar{\lambda} \ll \text{Tr}(\mathbf{V}_1) = \text{Tr}(\mathbf{V}_2)$, therefore the reshaped KME has a significantly smaller estimation error.
2. **Ability to handle dependent data.** Algorithm 1 applies to time series consisting of highly dependent data. The proof of Theorem 1 handles dependency by constructing a special matrix martingale and using the mixing properties of the Markov process to analyze its concentration.
3. **Tractable implementation.** Kernel-based methods usually require memorizing all the data and may be intractable in practice. Our approach is based on a finite number of features and only needs to low-dimensional computation. As pointed out by [RR08], one can approximate any shift-invariant kernel function using N features where N is linear with respect to the input dimension d . Therefore Algorithm 1 can be approximately implemented in $O(nd^2)$ time and $O(d^2)$ space.

3 Embedding States into Euclidean Space

In this section we want to learn low-dimensional representations of the state space Ω to capture the transition dynamics. We need following extra assumption that p can be fully represented in the kernel space.

Assumption 2. *The transition kernel belongs to the product Hilbert space, i.e., $p(\cdot | \cdot) \in \mathcal{H} \times \tilde{\mathcal{H}}$.*

For two arbitrary states $x, y \in \Omega$, we consider their distance given by

$$\text{dist}(x, y) := \|p(\cdot | x) - p(\cdot | y)\|_{L^2} = \left(\int (p(z|x) - p(z|y))^2 dz \right)^{1/2}. \quad (3)$$

Eq. (3) is known as the diffusion distance [NLCK06]. It measures the similarity between future paths of two states. We are motivated by the diffusion map approach for dimension reduction [LL06, CKL⁺08, KSM18]. Diffusion map refers to the leading eigenfunctions of the transfer operator of a reversible dynamical system. We will generalize it to nonreversible processes and feature spaces.

For simplicity of presentation, we assume without loss of generality that $\{\Phi_i\}_{i=1}^N$ and $\{\tilde{\Phi}_i\}_{i=1}^N$ are $L_2(\pi)$ and L_2 orthogonal bases of \mathcal{H} and $\tilde{\mathcal{H}}$ respectively, with squared norms $\rho_1 \geq \dots \geq \rho_N$ and $\tilde{\rho}_1 \geq \dots \geq \tilde{\rho}_N$ respectively. Any given features can be orthogonalized to satisfy this condition. In particular, let the matrix $\mathbf{C} := \text{diag}[\rho_1, \dots, \rho_N]$, $\tilde{\mathbf{C}} := \text{diag}[\tilde{\rho}_1, \dots, \tilde{\rho}_N]$, it is easy to verify that $p(y|x) = \Phi(x)^T \mathbf{C}^{-1} \mathbf{P} \tilde{\mathbf{C}}^{-1} \tilde{\Phi}(y)$. Let $\mathbf{C}^{-1/2} \mathbf{P} \tilde{\mathbf{C}}^{-1/2} = \mathbf{U}^{(\rho)} \Sigma_{[1 \dots r]}^{(\rho)} \mathbf{V}^{(\rho)}$ be its SVD. We define the state embedding as

$$\Psi(x) := \left(\Phi(x)^T \mathbf{C}^{-1/2} \mathbf{U}^{(\rho)} \Sigma_{[1 \dots r]}^{(\rho)} \right)^T.$$

It is straightforward to verify that $\text{dist}(x, z) = \|\Psi(x) - \Psi(z)\|$. We propose to estimate Ψ in Algorithm 2.

Algorithm 2: Learning State Embedding

Input: $\{X_1, \dots, X_n\}, r$;

Get $\hat{\mathbf{P}}$ from (2), compute SVD $\hat{\mathbf{U}}^{(\rho)} \hat{\Sigma}^{(\rho)} \hat{\mathbf{V}}^{(\rho)} = \mathbf{C}^{-1/2} \hat{\mathbf{P}} \tilde{\mathbf{C}}^{-1/2}$;

Compute state embedding using first r singular pairs $\hat{\Psi}(x) = \left(\Phi(x)^T \mathbf{C}^{-1/2} \hat{\mathbf{U}}^{(\rho)} \hat{\Sigma}_{[1 \dots r]}^{(\rho)} \right)^T$;

Output: $x \mapsto \hat{\Psi}(x)$

Let $\widehat{dist}(x, z) := \|\hat{\Psi}(x) - \hat{\Psi}(z)\|$. We show that the estimated state embeddings preserve the diffusion distance with an additive distortion.

Theorem 2 (Maximum additive distortion of state embeddings). *Let Assumptions 1,2 hold. Let $L_{max} := \sup_{x \in \Omega} \Phi(x)^T \mathbf{C}^{-1} \Phi(x)$ and let κ be the condition number of $\sqrt{\pi(x)}p(y|x)$. For any $0 < \delta < 1$ and for all $x, z \in \Omega$, $|dist(x, z) - \widehat{dist}(x, z)|$ is upper bounded by:*

$$C \sqrt{\frac{L_{max}}{\rho_N \tilde{\rho}_N}} \left[\sqrt{2\kappa} + 1 \right] \left(\sqrt{\frac{t_{mix} \bar{\lambda} \log(2t_{mix} N / \delta)}{n}} + \frac{t_{mix} K_{max} \log(2t_{mix} N / \delta)}{3n} \right)$$

with probability at least $1 - \delta$ for some constant C .

Under Assumption 2, we can recover the full transition kernel from data by

$$\hat{p}(y|x) = \Phi(x)^T \mathbf{C}^{-1/2} \hat{\mathbf{U}}^{(\rho)} \hat{\Sigma}_{[1 \dots r]}^{(\rho)} (\hat{\mathbf{V}}^{(\rho)})^T \tilde{\mathbf{C}}^{-1/2} \tilde{\Phi}(y).$$

Theorem 3 (Recovering the transition density). *Let Assumptions 1,2 hold. For any $\delta \in (0, 1)$,*

$$\|p(\cdot|\cdot) - \hat{p}(\cdot|\cdot)\|_{L^2(\pi) \times L^2} \leq C \sqrt{\frac{r}{\rho_N \tilde{\rho}_N}} \left(\sqrt{\frac{t_{mix} \bar{\lambda} \log(2t_{mix} N / \delta)}{n}} + \frac{t_{mix} K_{max} \log(2t_{mix} N / \delta)}{3n} \right)$$

with probability at least $1 - \delta$ for some constant C .

Theorems 2,3 provide the first statistical guarantee for learning state embeddings and recovering the transition density for continuous-state low-rank Markov processes. The state embedding learned by Algorithm 2 can be represented in $O(Nr)$ space since Φ is priorly known. When Ω is finite and the feature map is identity, Theorem 3 nearly matches the the information-theoretical error lower bound given by [LWZ18].

4 Clustering States Using Diffusion Distances

We want to find a partition of the state space into m disjoint sets $\Omega_1 \dots \Omega_m$. The principle is if $x, y \in \Omega_i$ for some i , then $p(\cdot|x) \approx p(\cdot|y)$, meaning that states within the same set share similar future paths. This motivates us to study the following optimization problem, which has been considered in studies for dynamical systems [SS13],

$$\min_{\Omega_1, \dots, \Omega_m} \min_{q_1 \in \tilde{\mathcal{H}}, \dots, q_m \in \tilde{\mathcal{H}}} \sum_{i=1}^m \int_{\Omega_i} \pi(x) \|p(\cdot|x) - q_i(\cdot)\|_{L^2}^2 dx, \quad (4)$$

We assume without loss of generality that it admits a unique optimal solution, which we denote by $(\Omega_1^*, \dots, \Omega_m^*)$ and (q_1^*, \dots, q_m^*) . Under Assumption 2, each $q_i^*(\cdot)$ is a probability distribution and can be represented by right singular functions $\{v_k(\cdot)\}_{k=1}^r$ of $p(\cdot|\cdot)$ (Lemma 7 in Appendix). We propose the following state clustering method:

Algorithm 3: Learning metastable state clusters

Data: $\{X_1, \dots, X_n, r, m\}$

Use Alg. 2 to get state embedding $\hat{\Psi} : \Omega \mapsto \mathbb{R}^r$;

Solve k-means problem:

$$\min_{\Omega_1, \dots, \Omega_m} \min_{s_1, \dots, s_m \in \mathbb{R}^r} \sum_{i=1}^m \int_{\Omega_i} \pi(x) \|\hat{\Psi}(x) - s_i\|^2 dx;$$

Output: $\hat{\Omega}_1^* \dots \hat{\Omega}_m^*$

The k-means method uses the invariant measure π as a weight function. In practice if π is unknown, one can pick any reasonable measure and the theoretical bound can be adapted to that measure.

We analyze the performance of the state clustering method on finite data. Define the misclassification rate as

$$M(\hat{\Omega}_1^*, \dots, \hat{\Omega}_m^*) := \min_{\sigma} \sum_{j=1}^m \frac{\pi(\{x : x \in \Omega_j^*, i \notin \hat{\Omega}_{\sigma(j)}^*\})}{\pi(\Omega_j^*)},$$

where σ is taken over all possible permutations over $\{1, \dots, m\}$. The misclassification rate is always between 0 and m . We let $\Delta_1^2 := \min_k \min_{l \neq k} \pi(\Omega_k^*) \|q_l^* - q_k^*\|_{L^2}^2$ and let Δ_2^2 be the minimal value of (4).

Theorem 4 (Misclassification error bound for state clustering). *Let Assumptions 1,2 hold. Let κ be the condition number of $\sqrt{\pi(x)}p(y|x)$. If $\Delta_1 > 4\Delta_2$, then for any $0 < \delta < 1$ and $\epsilon > 0$, by letting*

$$n = \Theta\left(\frac{\kappa^2 r \bar{\lambda} t_{mix} \log(2t_{mix}N/\delta)}{\rho_N \bar{\rho}_N} \cdot \max\left\{\frac{1}{(\Delta_1 - 4\Delta_2)^2}, \frac{1}{\epsilon \Delta_1^2}, \frac{\Delta_2^2}{\epsilon^2 \Delta_1^4}\right\}\right),$$

we have $M(\hat{\Omega}_1^, \dots, \hat{\Omega}_m^*) \leq \frac{16\Delta_2^2}{\Delta_1^2} + \epsilon$ with probability at least $1 - \delta$.*

The full proof is given in Appendix. The condition $\Delta_1 > 4\Delta_2$ is a separability condition needed for finding the correct clusters with high probability, and $\frac{16\Delta_2^2}{\Delta_1^2}$ is non-vanishing misclassification error. In the case of reversible finite-state Markov process, the clustering problem is equivalent to finding the *optimal metastable m -full partition* given by $\operatorname{argmax}_{\Omega_1, \dots, \Omega_m} \sum_{k=1}^m p(\Omega_k | \Omega_i)$, where $p(\Omega_j | \Omega_i) := \frac{1}{\pi(\Omega_i)} \int_{x \in \Omega_i, y \in \Omega_j} \pi(x)p(y|x)dydx$ [ELVE08, SS13]. The optimal partition $(\Omega_1^*, \dots, \Omega_m^*)$ gives metastable sets that can be used to construct a reduced-order Markov state model [SS13]. In the more general case of nonreversible Markov chains, the proposed method will cluster states together if they share similar future paths. It provides an unsupervised learning method for state aggregation, which is a widely used heuristic for dimension reduction of control and reinforcement learning [BT96, SJJ95].

5 Experiments

5.1 Stochastic Diffusion Processes

We test the proposed approach on simulated diffusion processes of the form $dX_t = -\nabla V(X_t)dt + \sqrt{2}dB_t$, $X_t \in \mathbb{R}^d$, where $V(\cdot)$ is a potential function and $\{B_t\}_{t \geq 0}$ is the standard Brownian motion. For any interval $\tau > 0$, the discrete-time trajectory $\{X_{k\tau}\}_{k=1}^\infty$ is a Markov process. We apply the Euler method to generate sample path $\{X_{k\tau}\}_{k=1}^n$ according to the stochastic differential equation.

We use the Gaussian kernels $K(x, y) = \tilde{K}(x, y) = \frac{1}{(2\pi\sigma^2)^{d/2}} e^{-\frac{\|x-y\|_2^2}{2\sigma^2}}$ where $\sigma > 0$, and construct RKHS $\mathcal{H} = \tilde{\mathcal{H}}$ from $L^2(\pi)$. To get the features Φ , we generate 2000 random Fourier features $\mathbf{h} = [h_1, h_2, \dots, h_N]^\top$ such that $K(x, y) \approx \sum_{i=1}^N h_i(x)h_i(y)$ ([RR08]), and then orthogonalize \mathbf{h} to get Φ .

Comparison between reshaped and plain KME

We apply Algorithm 1 to find the reshaped KME $\hat{\mu}_p$ and compare its error with the plain KME $\tilde{\mu}_p$ given by (2). The experiment is performed on a four-well diffusion on \mathbb{R} , and we take rank $r = 4$. By orthogonalizing $N = 2000$ random Fourier features, we obtain $J = 82$ basis functions. Figure 5.1 shows that the reshaped KME consistently outperforms plain KME with varying sample sizes.

State clustering to reveal metastable structures

We apply the state clustering method to analyze metastable structures of a diffusion process whose potential function $V(x)$ is given by Figure 5.1 (a). We generate trajectories of length $n = 10^6$ and take the time interval to be $\tau = 0.1, 1, 5$ and 10 . We conduct the state embedding and clustering procedures with rank $r = 4$. Figure 5.1 (c)

shows the clustering results for $\tau = 1$ with a varying number of clusters. The partition results reliably reveal metastable sets, which are also known as invariance sets that characterize slow dynamics of this process. Figure 5.1 (d) shows the four-cluster results with varying values of τ , where the contours are based on diffusion distances to the centroid in each cluster. One can see that the diffusion distance contours are dense when τ takes small values. This is because, when τ is small, the state embedding method largely captures fast local dynamics. By taking τ to be larger values, the state embedding

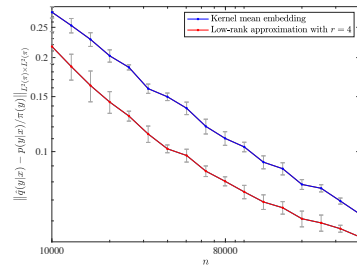


Figure 1: **Reshaped KME versus plain KME.** The error curve approximately satisfies a convergence rate of $n^{-1/2}$.

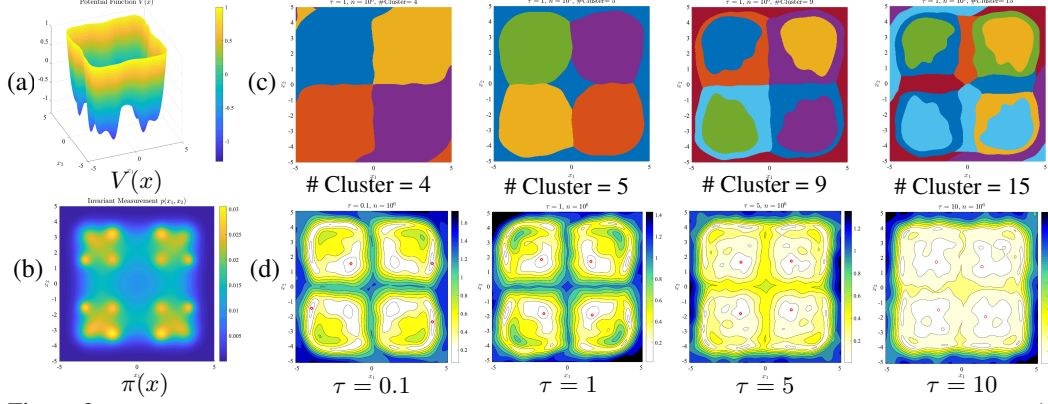


Figure 2: **Metastable state clusters learned from a stochastic diffusion process.** (a) Potential function $V(x)$ of the diffusion process. (b) Invariant measure $\pi(x)$. (c) State clusters based on a state embedding $\tilde{\Psi} : x \mapsto \mathbb{R}^4$. (d) Diffusion distance to the nearest cluster centroid (red dot) illustrated as contour plots.

method begins to capture slower dynamics, which corresponds to low-frequency transitions among the leading metastable sets.

5.2 DQN for Demon Attack

We test the state embedding method on the game trajectories of Demon Attack, an Atari 2600 game. In this game, demons appear in waves, move randomly and attack from above, where the player moves to dodge the bullets and shoots with a laser cannon. We train a Deep Q-Network using the architecture given by [MKS⁺15]. The DQN takes recent image frames of the game as input, processes them through three convolutional layers and two fully connected layers, and outputs a single value for each action, among which the action with the maximal value is chosen. Please refer to Appendix for more details on DQN training. In our experiment, we take the times series generated by the last hidden layer of a trained DQN when playing the game as our raw data. The raw data is a time series of length 47936 and dimension 512, comprising 130 game trajectories. We apply the state embedding method by approximating the Gaussian kernel with 200 random Fourier features. Then we obtain low-dimensional embeddings of the game states in \mathbb{R}^3 .

Before embedding vs. after embedding

Figure 3 visualizes the raw states and the state embeddings using t-SNE, a visualization tool to illustrate multi-dimensional data in two dimensions [VdM08]. In both plots, states that are mapped to nearby points tend to have similar “values” (expected future returns) as predicted by the DQN, as illustrated by colors of data points.

Comparing Figure 3(a) and (b), the raw state data are more scattered, while after embedding they exhibit clearer structures and fewer outliers. The markers \circ , \triangle , \diamond identify the same pair of game states before and after embedding. They suggest that the embedding method maps game states that are far apart from each other in their raw data to closer neighbors. It can be viewed as a form of compression. The experiment has been repeated multiple times. We consistently observe that state embedding leads to improved clusters and higher granularity in the t-SNE visualization.

Understanding state embedding from examples

Figure 4 illustrates three examples that were marked by \circ , \triangle , \diamond in Figure 3. In each example, we have a pair of game states that were far apart in their raw data but are close to each other after embedding. Also note the two images are visually not alike, therefore any representation learning method based on individual images alone will not consider them to be similar. Let us analyze these three examples:

- \circ : Both streaming lasers (purple) are about to destroy a demon and generate a reward; Both cannons are moving towards the left end.
- \triangle : In both images, two new demons are emerging on top of the cannon to join the battle and there is an even closer enemy, leading to future dangers and potential rewards.
- \diamond : Both cannons are waiting for more targets to appear, and they are both moving towards the center from opposite sides.

These examples suggest that state embedding is able to identify states as similar *if they share similar near-future events and values*, even though they are visually dissimilar and distant from each other in their raw data.

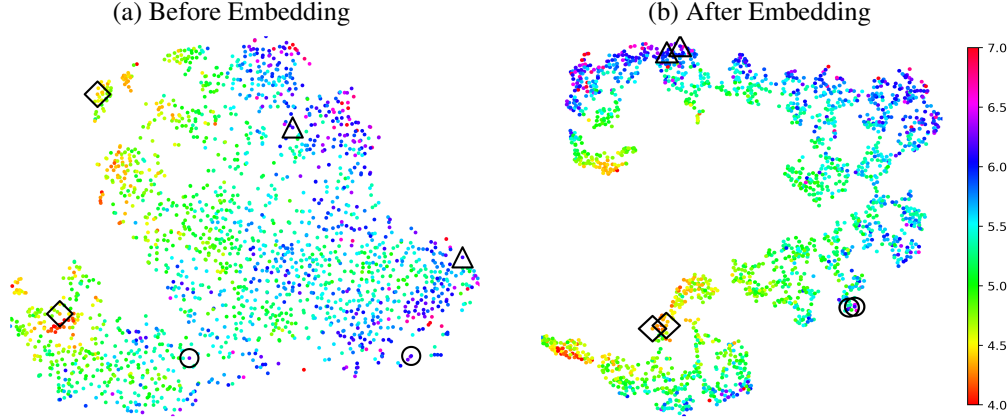


Figure 3: **Visualization of game states before and after embedding in t-SNE plots.** The raw data is a time series of 512 dimensions, which generated by the last hidden layer by the DQN while it is playing Demon Attack. State embeddings are computed from the raw time series using a Gaussian kernel with 200 random Fourier features. Game states are colored by the “value” of the state as predicted by the DQN. The markers \circ , \triangle , \diamond identify the same pair of game states before and after embedding. Comparing (a) and (b), state embedding improves the granularity of clusters and reveals more structures of the data.

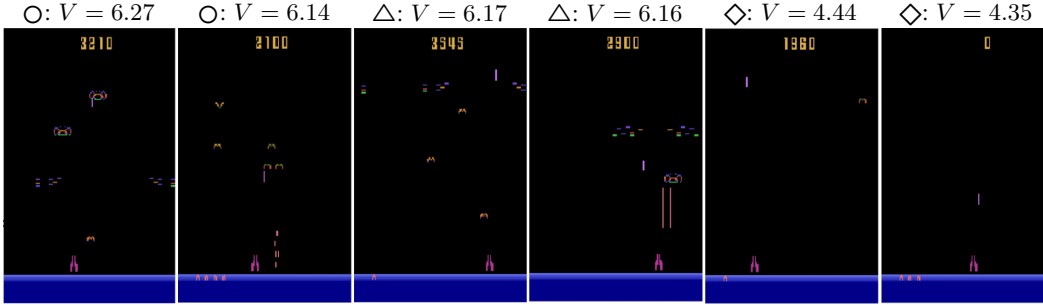


Figure 4: **Pairs of game states that are close after embedding (\circ , \triangle , \diamond in Figure 3).** Within each pair, the two states share similar “V” values as predicted by the DQN, but they were not close in the raw data and are visually dissimilar. \circ : Both streaming lasers (purple) are about to destroy a demon and generate a reward; Both cannons are moving towards the left end. \triangle : In both images, two new demons are emerging on top of the cannon to join the battle and there is an even closer enemy, leading to future dangers and potential rewards. \diamond : Both cannons are waiting for more targets to appear, and they are both moving towards the center from opposite sides. The examples above suggest that state embedding is able to identify states as similar if they share similar near-future paths and values.

Summary and Future Work

The experiments validate our theory and lead to interesting discoveries: estimated state embedding captures what would happen in the future conditioned on the current state. Thus the state embedding can be useful to decision makers in terms of gaining insights into the underlying logic of the game, thereby helping them to make better predictions and decisions.

Our methods are inspired by dimension reduction methods from scientific computing and they further leverage the low-rankness of the transition kernel to reduce estimation error and find compact state embeddings. Our theorems provide the basic statistical theory on state embedding/clustering from finite-length dependent time series. They are the first theoretical results known for continuous-state Markov process. We hope our results would motivate more work on this topic and lead to broader applications in scientific data analysis and machine learning. A natural question to ask next is how can one use state embedding to make control and reinforcement learning more efficient. This is a direction for future research.

References

- [BNVB13] M. G. Bellemare, Y. Naddaf, J. Veness, and M. Bowling. The arcade learning environment: An evaluation platform for general agents. Journal of Artificial Intelligence Research, 47:253–279, 2013.
- [BSB⁺15] Wendelin Böhmer, Jost Tobias Springenberg, Joschka Boedecker, Martin Riedmiller, and Klaus Obermayer. Autonomous learning of state representations for control. Künstliche Intelligenz, 29(4):1–10, 2015.
- [BT96] Dimitri P Bertsekas and John N Tsitsiklis. Neuro-dynamic programming, volume 5. Athena Scientific Belmont, MA, 1996.
- [BTA04] Alain A Berline and Christine Thomas-Agnan. Reproducing Kernel Hilbert Spaces in Probability and Statistics. Kluwer Academic Publishers, 2004.
- [CKL⁺08] Ronald R. Coifman, Ioannis G. Kevrekidis, Stéphane Lafon, Mauro Maggioni, and Boaz Nadler. Diffusion maps, reduction coordinates, and low dimensional representation of stochastic systems. SIAM Journal on Multiscale Modeling and Simulation, 7(2):852–864, 2008.
- [DKW19] Yaqi Duan, Zheng Tracy Ke, and Mengdi Wang. State aggregation learning from markov transition data. Conference on Neural Information Processing Systems (NeurIPS), 2019.
- [ELVE08] Weinan E, Tiejun Li, and Eric Vanden-Eijnden. Optimal partition and effective dynamics of complex networks. Proceedings of the National Academy of Sciences, 105(23):7907–7912, 2008.
- [Går54] Lars Gårding. On the asymptotic distribution of the eigenvalues and eigenfunctions of elliptic differential operators. Mathematica Scandinavica, pages 237–255, 1954.
- [GLB⁺12] Steffen Grünewälder, Guy Lever, Luca Baldassarre, Massimiliano Pontil, and Arthur Gretton. Modelling transition dynamics in mdps with rkhs embeddings. International Conference on Machine Learning, 2012.
- [KAL16] Akshay Krishnamurthy, Alekh Agarwal, and John Langford. Pac reinforcement learning with rich observations. In Advances in Neural Information Processing Systems, pages 1840–1848, 2016.
- [KB15] Diederik P. Kingma and Jimmy Ba. Adam: A method for stochastic optimization. In 3rd International Conference on Learning Representations, ICLR 2015, San Diego, CA, USA, May 7-9, 2015, Conference Track Proceedings, 2015.
- [KKS16] Stefan Klus, Péter Koltai, and Christof Schütte. On the numerical approximation of the peronfrobenius and koopman operator. Journal of Computational Dynamics, 3(1):51–79, 2016.
- [KNK⁺18] Stefan Klus, Feliks Nüske, Péter Koltai, Hao Wu, Ioannis Kevrekidis, Christof Schütte, and Frank Noé. Data-driven model reduction and transfer operator approximation. Journal of Nonlinear Science, 28(3):985–1010, 2018.
- [KSM18] Stefan Klus, Ingmar Schuster, and Krikamol Muandet. Eigendecompositions of transfer operators in reproducing kernel hilbert spaces. arXiv preprint arXiv:1712.01572, 2018.
- [Lac07] Claire Lacour. Estimation non paramtrique adaptative pour les chanes de Markov et les chanes de Markov caches. PhD thesis, Ph.D. Thesis, UNIVERSITE PARIS DESCARTES, 2007.
- [LL06] Stéphane Lafon and Ann Lee. Diffusion maps and coarse-graining: A unified framework for dimensionality reduction, graph partitioning, and data set parameterization. IEEE Trans. on Pattern Analysis and Machine Intelligence, 29(9):1393–1403, 2006.
- [LP17] David A Levin and Yuval Peres. Markov chains and mixing times, volume 107. American Mathematical Soc., 2017.
- [LP18] Matthias Löffler and Antoine Picard. Spectral thresholding for the estimation of markov chain transition operators. arXiv preprint arXiv:1808.08153, 2018.
- [LPMST15] David Lopez-Paz, Krikamol Muandet, Bernhard Scholkopf, and Ilya Tolstikhini. Towards a learning theory of cause-effect inference. International Conference on Machine Learning, 2015.
- [LR⁺15] Jing Lei, Alessandro Rinaldo, et al. Consistency of spectral clustering in stochastic block models. The Annals of Statistics, 43(1):215–237, 2015.

- [LWZ18] Xudong Li, Mengdi Wang, and Anru Zhang. Estimation of markov chain via rank-constrained likelihood. International Conference on Machine Learning, 2018.
- [MFSS17] Kirkamol Muandet, Kenji Fukumizu, Bharath Sriperumbudur, and Bernhard Schölkopf. Kernel mean embedding of distributions: A review and beyond. Foundations and Trends in Machine Learning, 10(1-2):1–141, 2017.
- [MKS⁺15] Volodymyr Mnih, Koray Kavukcuoglu, David Silver, Andrei A. Rusu, Joel Veness, Marc G. Bellemare, Alex Graves, Martin Riedmiller, Andreas K. Fidjeland, Georg Ostrovski, Stig Petersen, Charles Beattie, Amir Sadik, Ioannis Antonoglou, Helen King, Dharshan Kumaran, Daan Wierstra, Shane Legg, and Demis Hassabis. Human-level control through deep reinforcement learning. Nature, 518:529–533, 2015.
- [NLCK06] Boaz Nadler, Stéphane Lafon, Ronald R. Coifman, and Ioannis G. Kevrekidis. Diffusion maps, spectral clustering and eigenfunctions of fokker-planck operators. In Advances in neural information processing systems, pages 955–962, 2006.
- [RR08] Ali Rahimi and Benjamin Recht. Random features for large-scale kernel machines. In Advances in neural information processing systems, pages 1177–1184, 2008.
- [RZMC11] Mary A Rohrdanz, Wenwei Zheng, Mauro Maggioni, and Cecilia Clementi. Determination of reaction coordinates via locally scaled diffusion map. The Journal of chemical physics, 134(12):03B624, 2011.
- [Sar14] Mathieu Sart. Estimation of the transition density of a markov chain. In Annales de l’IHP Probabilités et statistiques, volume 50, pages 1028–1068, 2014.
- [SGSS07] Alex Smola, Arthur Gretton, Le Song, and Schölkopf. A hilbert space embedding for distributions. In International Conference on Algorithmic Learning Theory, 2007.
- [SHSF09] Le Song, Jonathan Huang, Alex Smola, and Kenji Fukumizu. Hilbert space embeddings of conditional distributions with applications to dynamical systems. International Conference on Machine Learning, 2009.
- [SJJ95] Satinder P Singh, Tommi Jaakkola, and Michael I Jordan. Reinforcement learning with soft state aggregation. In Advances in neural information processing systems, pages 361–368, 1995.
- [SNL⁺11] Christof Schütte, Frank Noe, Jianfeng Lu, Macro Sarich, and Eric Vanden-Eijnden. Markov state models based on milestoning. The Journal of Chemical Physics, 134(20):204105, 2011.
- [SS13] Christof Schütte and Marco Sarich. Metastability and Markov State Models in Molecular Dynamics: Modelling, Analysis, Algorithm Approach, volume 24. American Mathematical Soc., 2013.
- [Tro11] Joel A Tropp. Freedmans inequality for matrix martingales. Electron. Commun. Probab, 16:262–270, 2011.
- [VdM08] G. Van der Maaten, Hinton. Visualizing high-dimensional data using t-sne. Journal of Machine Learning Research, 9(Nov):2579–2605, 2008.
- [Wed72] Per-Ake Wedin. Perturbation bounds in connection with singular value decomposition. BIT Numerical Mathematics, 12(1):99–111, 1972.
- [Wey12] Hermann Weyl. Das asymptotische verteilungsgesetz der eigenwerte linearer partieller differentialgleichungen (mit einer anwendung auf die theorie der hohlraumstrahlung). Mathematische Annalen, 71(4):441–479, 1912.
- [Yak79] Sidney Yakowitz. Nonparametric estimation of markov transition func- tions. The Annals of Statistics, 7(3):671–679, 1979.
- [ZC18] Anru Zhang and Tony Cai. Rate-optimal perturbation bounds for singular subspaces with applications to high-dimensional statistics. Annals of Statistics, 46:60–89, 2018.
- [ZW18] Anru Zhang and Mengdi Wang. Spectral state compression of markov processes. arXiv preprint arXiv:1802.02920, 2018.

Appendices

A Proofs for Section 3

A.1 Technical Lemmas

Lemma 5 (Theorem 1 of [LPMST15]). *Suppose $\{(X_i, X'_i)\}_{i=1}^n \stackrel{i.i.d.}{\sim} p(\cdot, \cdot)$, assume that $\|f \otimes g\|_\infty \leq 1$ for all $f \otimes g \in \mathcal{H} \times \tilde{\mathcal{H}}$ with $\|f \otimes g\|_{\mathcal{H} \times \tilde{\mathcal{H}}} \leq 1$. Then with probability at least $1 - \delta$:*

$$\|\mu_p - \hat{\mu}_p\|_{\mathcal{H} \times \tilde{\mathcal{H}}} \leq 2\sqrt{\frac{\mathbb{E}_{(X,Y) \sim p}[K(X,X)\tilde{K}(Y,Y)]}{n}} + \sqrt{\frac{2\log(1/\delta)}{n}}.$$

Proof. See [LPMST15] for detailed proof. □

Lemma 6. *Under Assumption 1, the projection matrix*

$$\mathbf{P} = \int \pi(x)p(y|x)\Phi(x)\tilde{\Phi}(y)^T dx dy$$

has rank at most r .

Proof. We define $N \times 1$ vectors \vec{u}_k and \vec{v}_k as:

$$\vec{u}_k := \int \pi(x)u_k(x)\Phi(x)dx, \quad (5)$$

$$\vec{v}_k := \int v_k(y)\tilde{\Phi}(y)dy. \quad (6)$$

Then under Assumption 1, we can write:

$$\mathbf{P} = \int \pi(x)p(y|x)\Phi(x)\tilde{\Phi}(y)^T dx dy \quad (7)$$

$$= \sum_{k=1}^r \int \sigma_k \pi(x)u_k(x)v_k(y)\Phi(x)\tilde{\Phi}(y)dy \quad (8)$$

$$= \sum_{k=1}^r \sigma_k \vec{u}_k \vec{v}_k^T. \quad (9)$$

□

Lemma 7. *Suppose that $K(x, u) = \Phi(x)^T \Phi(u)$, $\tilde{K}(y, v) = \tilde{\Phi}(v)^T \tilde{\Phi}(y)$. With \mathbf{P} given by*

$$\mathbf{P} = \int p(x, y)\Phi(x)\tilde{\Phi}(y)^T dx dy.$$

We can represent KME of joint distribution $\mu_p(u, v)$ as:

$$\mu_p(x, y) = \int K(x, u)\tilde{K}(y, v)p(u, v)dudv = \Phi(x)^T \mathbf{P} \tilde{\Phi}(y).$$

Proof. By definition of KME for $p(u, v)$ into $\mathcal{H} \times \tilde{\mathcal{H}}$, we have:

$$\mu_p(x, y) = \int K(x, u)\tilde{K}(y, v)p(u, v)dudv.$$

We then write kernels in terms of features and get $K(x, u) = \Phi(x)^T \Phi(u)$, $\tilde{K}(y, v) = \tilde{\Phi}(v)^T \tilde{\Phi}(y)$. Plugging this into the definition of KME we get:

$$\mu_p(x, y) = \int K(x, u)\tilde{K}(y, v)p(u, v)dudv \quad (10)$$

$$= \int \Phi(x)^T \Phi(u)\tilde{\Phi}(v)^T \Phi(y)p(u, v)dudv \quad (11)$$

$$= \Phi(x)^T \left(\int p(u, v)\Phi(u)\tilde{\Phi}(v)^T dudv \right) \Phi(y) \quad (12)$$

$$= \Phi(x)^T \mathbf{P} \Phi(y). \quad (13)$$

□

Lemma 8. Consider the KME of $p(\cdot|\cdot)$ into $\mathcal{H} \times \tilde{\mathcal{H}}$ where \mathcal{H} has kernel $K(x, y)$ and $\tilde{\mathcal{H}}$ has kernel $\tilde{K}(x, y)$, $K(x, y) = \Phi(x)^T \Phi(y)$ and $\tilde{K}(x, y) = \tilde{\Phi}(x)^T \tilde{\Phi}(y)$. Let $\mathbf{V}_1 = \mathbb{E}_{(X, Y) \sim p}[\Phi(X)\Phi(X)^T \tilde{K}(Y, Y)]$ and $\mathbf{V}_2 = \mathbb{E}_{(X, Y) \sim p}[K(X, X)\tilde{\Phi}(Y)\tilde{\Phi}(Y)^T]$, $\bar{\lambda} = \max\{\lambda_{\max}(\mathbf{V}_1), \lambda_{\max}(\mathbf{V}_2)\}$. Let $\tau(\epsilon) := \min\{t \mid TV(P^t(\cdot|x), \pi(\cdot)) \leq \epsilon, \forall x \in \Omega\}$ denote the mixing time. Let $\epsilon > 0$, $\alpha(\epsilon) = \tau(\frac{\epsilon}{2K_{\max}} \wedge \frac{\bar{\lambda}}{K_{\max}^2}) + 1$, then:

$$\mathbb{P}(\|\hat{\mathbf{P}} - \mathbf{P}\| \geq \epsilon) \leq 2\alpha(\epsilon)N \exp\left(-\frac{n\epsilon^2/8}{2\alpha(\epsilon)\bar{\lambda} + \epsilon\alpha(\epsilon)K_{\max}/6}\right). \quad (14)$$

For any $0 < \delta < 1$, we have

$$\|\mathbf{P} - \hat{\mathbf{P}}\| \leq C \left(\sqrt{\frac{t_{\max}\bar{\lambda} \log(2t_{\max}N/\delta)}{n}} + \frac{t_{\max}K_{\max} \log(2t_{\max}N/\delta)}{3n} \right) \quad (15)$$

with probability at least $1 - \delta$, where C is an universal constant.

Proof. Let $n_0 = \lfloor n/\alpha \rfloor$. Define

$$\hat{\mathbf{P}}_t := \Phi(X_{t-1})\tilde{\Phi}(X_t)^T \quad \text{for } t = 2, 3, \dots, n,$$

and the “thin” sequence:

$$\check{\mathbf{P}}_k^{(l)} := \hat{\mathbf{P}}_{k\alpha+l} - \mathbb{E}(\hat{\mathbf{P}}_{k\alpha+l} | \hat{\mathbf{P}}_{(k-1)\alpha+l}). \quad (16)$$

We first bound $\|\hat{\mathbf{P}}_{k\alpha+l}\|$:

$$\|\hat{\mathbf{P}}_{k\alpha+l}\| = \sup_{\substack{\|\mathbf{v}\|_{\ell_2} \leq 1 \\ \|\mathbf{u}\|_{\ell_2} \leq 1}} \mathbf{v}^T \hat{\mathbf{P}}_{k\alpha+l} \mathbf{u} \quad (17)$$

$$= \sup_{\substack{\|\mathbf{v}\|_{\ell_2} \leq 1 \\ \|\mathbf{u}\|_{\ell_2} \leq 1}} \sum_{i,j=1}^N \mathbf{v}_i \Phi_i(X_{k\alpha+l-1}) \tilde{\Phi}_j(X_{k\alpha+l}) \mathbf{u}_j \quad (18)$$

$$\leq K_{\max}. \quad (19)$$

In the last inequality we use the fact that for any vector \mathbf{v} with $\|\mathbf{v}\|_{\ell_2} \leq 1$,

$$\sum_{i=1}^N \mathbf{v}_i \Phi_i(x) \leq \|\mathbf{v}\|_{\ell_2} \|\Phi(x)\|_{\ell_2} \leq \sqrt{K(x, x)} \leq K_{\max}^{1/2}, \quad (20)$$

where we used $\|\Phi(x)\|_{\ell_2}^2 = K(x, x)$ and the definition of K_{\max} . Similar argument applies for $\sum_{j=1}^N \mathbf{u}_j \tilde{\Phi}_j(x)$. Hence $\|\mathbb{E}(\hat{\mathbf{P}}_{k\alpha+l} | \hat{\mathbf{P}}_{(k-1)\alpha+l})\| \leq \mathbb{E}(\|\hat{\mathbf{P}}_{k\alpha+l}\| | \hat{\mathbf{P}}_{(k-1)\alpha+l}) \leq K_{\max}$ and we have:

$$\|\check{\mathbf{P}}_k^{(l)}\| \leq 2K_{\max}. \quad (21)$$

Let $p^\alpha(x|x_{(k-1)\alpha+l})$ be the $(\alpha-1)$ -step transition density starting from $x_{(k-1)\alpha+l}$. We use “ \cdot ” to denote dot product of two vectors, then we have:

$$(\hat{\mathbf{P}}_{k\alpha+l} \hat{\mathbf{P}}_{k\alpha+l}^T)_{ij} := (\hat{\mathbf{P}}_{k\alpha+l})_{[i,:]} \cdot (\hat{\mathbf{P}}_{k\alpha+l})_{[j,:]} \quad (22)$$

$$= \sum_{p=1}^N \Phi_i(X_{k\alpha+l-1}) \Phi_j(X_{k\alpha+l-1}) \tilde{\Phi}_p^2(X_{k\alpha+l}). \quad (23)$$

Taking conditional expectation yields:

$$\mathbb{E}\left(\hat{\mathbf{P}}_{k\alpha+l} \hat{\mathbf{P}}_{k\alpha+l}^T | x_{(k-1)\alpha+l}\right)_{ij} = \int \Phi_i(x) \Phi_j(x) p^\alpha(x|x_{(k-1)\alpha+l}) p(y|x) \sum_{p=1}^N \tilde{\Phi}_p^2(y) dx dy \quad (24)$$

$$= \int \Phi_i(x) \Phi_j(x) p^\alpha(x|x_{(k-1)\alpha+l}) p(y|x) \tilde{K}(y, y) dx dy. \quad (25)$$

We can write

$$\mathbb{E}\left(\hat{\mathbf{P}}_{k\alpha+l} \hat{\mathbf{P}}_{k\alpha+l}^T | x_{(k-1)\alpha+l}\right)_{ij} = \left(\mathbb{E}\left(\hat{\mathbf{P}}_{k\alpha+l} \hat{\mathbf{P}}_{k\alpha+l}^T | x_{(k-1)\alpha+l}\right) - \mathbf{V}_1\right)_{ij} + (\mathbf{V}_1)_{ij} \quad (26)$$

$$= \int \Phi_i(x) \Phi_j(x) \left(p^\alpha(x|x_{(k-1)\alpha+l}) - \pi(x)\right) p(y|x) \tilde{K}(y, y) dx dy \quad (27)$$

$$+ \int \Phi_i(x) \Phi_j(x) \pi(x) p(y|x) \tilde{K}(y, y) dx dy. \quad (28)$$

Therefore:

$$\|\mathbb{E}\left(\hat{\mathbf{P}}_{k\alpha+l}\hat{\mathbf{P}}_{k\alpha+l}^T|x_{(k-1)\alpha+l}\right)\| \quad (29)$$

$$= \left\| \left(\mathbb{E}\left(\hat{\mathbf{P}}_{k\alpha+l}\hat{\mathbf{P}}_{k\alpha+l}^T|x_{(k-1)\alpha+l}\right) - \mathbf{V}_1 \right) + \mathbf{V}_1 \right\| \quad (30)$$

$$\leq \left\| \left(\mathbb{E}\left(\hat{\mathbf{P}}_{k\alpha+l}\hat{\mathbf{P}}_{k\alpha+l}^T|x_{(k-1)\alpha+l}\right) - \mathbf{V}_1 \right) \right\| + \|\mathbf{V}_1\| \quad (31)$$

$$= \underbrace{\sup_{\substack{\|\mathbf{v}\|_{\ell_2} \leq 1, \\ \|\mathbf{u}\|_{\ell_2} \leq 1}} \int [\mathbf{v}^T \Phi(x)] [\mathbf{u}^T \Phi(x)] p^\alpha(x|x_{(k-1)\alpha+l} - \pi(x)) p(y|x) \tilde{K}(y, y) dy dx}_{T_1} + \|\mathbf{V}_1\|. \quad (32)$$

By (20) we have $\|\mathbf{v}^T \Phi\|_\infty \leq K_{max}^{1/2}$ and similarly $\|\mathbf{u}^T \Phi\|_\infty \leq K_{max}^{1/2}$, using definition of K_{max} we have $\tilde{K}(y, y) \leq K_{max}$, we bound the term T_1 by:

$$T_1 = \sup_{\substack{\|\mathbf{v}\|_{\ell_2} \leq 1, \\ \|\mathbf{u}\|_{\ell_2} \leq 1}} \int [\mathbf{v}^T \Phi(x)] [\mathbf{u}^T \Phi(x)] (p^\alpha(x|x_{(k-1)\alpha+l}) - \pi(x)) p(y|x) \tilde{K}(y, y) dx dy \quad (33)$$

$$\leq K_{max}^2 \int |p^\alpha(x|x_{(k-1)\alpha+l}) - \pi(x)| dx \quad (34)$$

$$\leq \bar{\lambda}, \quad (35)$$

where in the last inequality we use the definition of $\alpha(\epsilon)$. By definition of $\bar{\lambda}$ we have $\|\mathbf{V}_1\| \leq \bar{\lambda}$, therefore by (32) we get:

$$\|\mathbb{E}\left(\hat{\mathbf{P}}_{k\alpha+l}\hat{\mathbf{P}}_{k\alpha+l}^T|x_{(k-1)\alpha+l}\right)\| \leq 2\bar{\lambda}. \quad (36)$$

Similarly, we have:

$$\|\mathbb{E}\left(\hat{\mathbf{P}}_{k\alpha+l}^T\hat{\mathbf{P}}_{k\alpha+l}|x_{(k-1)\alpha+l}\right)\| \leq 2\bar{\lambda}. \quad (37)$$

Combining the fact that:

$$0 \preceq \mathbb{E}\left(\check{\mathbf{P}}_k^{(l)}(\check{\mathbf{P}}_k^{(l)})^T|\check{\mathbf{P}}_{k-1}^{(l)}\right) \quad (38)$$

$$= \mathbb{E}\left(\hat{\mathbf{P}}_{k\alpha+l}\hat{\mathbf{P}}_{k\alpha+l}^T|x_{(k-1)\alpha+l}\right) - \mathbb{E}\left(\hat{\mathbf{P}}_{k\alpha+l}|x_{(k-1)\alpha+l}\right)\mathbb{E}\left(\hat{\mathbf{P}}_{k\alpha+l}|x_{(k-1)\alpha+l}\right) \quad (39)$$

$$\preceq \mathbb{E}\left(\hat{\mathbf{P}}_{k\alpha+l}\hat{\mathbf{P}}_{k\alpha+l}^T|x_{(k-1)\alpha+l}\right), \quad (40)$$

we have

$$\|\mathbb{E}\left(\check{\mathbf{P}}_k^{(l)}(\check{\mathbf{P}}_k^{(l)})^T|\check{\mathbf{P}}_{k-1}^{(l)}\right)\| \leq \|\mathbb{E}\left(\hat{\mathbf{P}}_{k\alpha+l}\hat{\mathbf{P}}_{k\alpha+l}^T|x_{(k-1)\alpha+l}\right)\| \leq 2\bar{\lambda}. \quad (41)$$

Similar argument yields:

$$\|\mathbb{E}\left((\check{\mathbf{P}}_k^{(l)})^T\check{\mathbf{P}}_k^{(l)}|\check{\mathbf{P}}_{k-1}^{(l)}\right)\| \leq 2\bar{\lambda}. \quad (42)$$

Therefore for $1 \leq k \leq n_0, 1 \leq l \leq \alpha$:

$$\max \left\{ \|\mathbb{E}\left(\check{\mathbf{P}}_k^{(l)}(\check{\mathbf{P}}_k^{(l)})^T|\check{\mathbf{P}}_{k-1}^{(l)}\right)\|, \|\mathbb{E}\left((\check{\mathbf{P}}_k^{(l)})^T\check{\mathbf{P}}_k^{(l)}|\check{\mathbf{P}}_{k-1}^{(l)}\right)\| \right\} \leq 2\bar{\lambda}. \quad (43)$$

The norm of predictable quadratic variation process of the matrix martingale $\{\check{\mathbf{P}}_k^{(l)}\}_{k=1}^{n_0}$ can be bounded by:

$$\left\| \sum_{k=1}^{n_0} \mathbb{E}\left(\check{\mathbf{P}}_k^{(l)}(\check{\mathbf{P}}_k^{(l)})^T|\check{\mathbf{P}}_{k-1}^{(l)}\right) \right\| \leq \sum_{k=1}^{n_0} \|\mathbb{E}\left(\check{\mathbf{P}}_k^{(l)}(\check{\mathbf{P}}_k^{(l)})^T|\check{\mathbf{P}}_{k-1}^{(l)}\right)\| \leq 2n_0\bar{\lambda}, \quad (44)$$

$$\left\| \sum_{k=1}^{n_0} \mathbb{E}\left((\check{\mathbf{P}}_k^{(l)})^T\check{\mathbf{P}}_k^{(l)}|\check{\mathbf{P}}_{k-1}^{(l)}\right) \right\| \leq \sum_{k=1}^{n_0} \|\mathbb{E}\left((\check{\mathbf{P}}_k^{(l)})^T\check{\mathbf{P}}_k^{(l)}|\check{\mathbf{P}}_{k-1}^{(l)}\right)\| \leq 2n_0\bar{\lambda}. \quad (45)$$

By Matrix Freedman Inequality [Tro11], we have:

$$\mathbb{P}(\|\frac{1}{n_0} \sum_{k=1}^{n_0} \hat{\mathbf{P}}_k^{(l)}\| \geq \epsilon/2) \leq 2N \exp(-\frac{(\epsilon n_0)^2/8}{2n_0\bar{\lambda} + \epsilon K_{\max} n_0/6}). \quad (46)$$

Next we note that:

$$\left(\mathbb{E}(\hat{\mathbf{P}}_{k\alpha+l}|x_{(k-1)\alpha+l}) - \mathbf{P} \right)_{i,j} = \int \Phi_i(x) \tilde{\Phi}_j(y) p(y|x) (p^\alpha(x|x_{(k-1)\alpha+l}) - \pi(x)) dx dy, \quad (47)$$

$$\begin{aligned} & \|\mathbb{E}(\hat{\mathbf{P}}_{k\alpha+l}|x_{(k-1)\alpha+l}) - \mathbf{P}\| \\ &= \sup_{\substack{\|\mathbf{v}\|_{\ell_2} \leq 1 \\ \|\mathbf{u}\|_{\ell_2} \leq 1}} \mathbf{v}^T \left(\mathbb{E}(\hat{\mathbf{P}}_{k\alpha+l}|x_{(k-1)\alpha+l}) - \mathbf{P} \right) \mathbf{u} \end{aligned} \quad (48)$$

$$= \sup_{\substack{\|\mathbf{v}\|_{\ell_2} \leq 1 \\ \|\mathbf{u}\|_{\ell_2} \leq 1}} \int [\mathbf{v}^T \Phi(x)] [\mathbf{u}^T \tilde{\Phi}(y)] p(y|x) \left(p^\alpha(x|x_{(k-1)\alpha+l}) - \pi(x) \right) dx dy \quad (49)$$

$$\leq K_{\max} \int |p^\alpha(x|x_{(k-1)\alpha+l}) - \pi(x)| dx \quad (50)$$

$$\leq \epsilon/2, \quad (51)$$

where we used definition of mixing-time $\alpha(\epsilon)$ to get last inequality. Then combining (46) and (51) we get:

$$\mathbb{P}(\|\frac{1}{n_0} \sum_{k=1}^{n_0} \hat{\mathbf{P}}_{k\alpha+l} - \mathbf{P}\| \geq \epsilon) \leq 2N \exp(-\frac{(\epsilon n_0)^2/8}{2n_0\bar{\lambda} + \epsilon K_{\max} n_0/6}). \quad (52)$$

Using union bound we get:

$$\mathbb{P}(\|\hat{\mathbf{P}} - \mathbf{P}\| \geq \epsilon) = \mathbb{P}\left(\|\frac{1}{\alpha} \sum_{l=1}^{\alpha} \frac{1}{n_0} \sum_{k=1}^{n_0} \mathbf{P}_{k\alpha+l} - \mathbf{P}\| \geq \epsilon\right) \quad (53)$$

$$\leq \mathbb{P}\left(\max_{1 \leq l \leq \alpha} \|\frac{1}{n_0} \sum_{k=1}^{n_0} \mathbf{P}_{k\alpha+l} - \mathbf{P}\| \geq \epsilon\right) \quad (54)$$

$$\leq \alpha(\epsilon) \max_{1 \leq l \leq \alpha} \mathbb{P}\left(\|\frac{1}{n_0} \sum_{k=1}^{n_0} \mathbf{P}_{k\alpha+l} - \mathbf{P}\| \geq \epsilon\right) \quad (55)$$

$$\leq 2\alpha(\epsilon)N \exp(-\frac{n\epsilon^2/8}{2\bar{\lambda}\alpha(\epsilon) + \epsilon K_{\max}\alpha(\epsilon)/6}). \quad (56)$$

To get Eqn.(15) from (14), we let $u = \log(\delta)$ and write ϵ using u , then we need:

$$\log(2\alpha(\epsilon)N) - \frac{n\epsilon^2/8}{\alpha(\epsilon)(2\bar{\lambda} + \epsilon K_{\max}/6)} \leq u, \quad (57)$$

using the fact that $\alpha(\epsilon)$ grows logarithmically (Lemma 5 in [ZW18]) and solve the above inequality for ϵ , we get (15). \square

Lemma 9. Under Assumption 1, let \mathbf{V} and $\tilde{\mathbf{V}}$ be the right singular matrix of \mathbf{P} and $\tilde{\mathbf{P}}$ respectively, then we have:

$$\inf_{\mathbf{O} \in \mathcal{O}_{r \times r}} \|\mathbf{VO} - \tilde{\mathbf{V}}\| \leq \frac{C}{\sigma_r(\mathbf{P})} \left(\sqrt{\frac{t_{mix}\bar{\lambda} \log(2t_{mix}N/\delta)}{n}} + \frac{t_{mix}K_{\max} \log(2t_{mix}N/\delta)}{3n} \right) \quad (58)$$

with probability at least $1 - \delta$, \mathcal{O} is the set of all $r \times r$ orthogonal matrices.

Proof. By Lemma.1 of [ZC18], we know:

$$\inf_{\mathbf{O} \in \mathcal{O}_{r \times r}} \|\mathbf{VO} - \tilde{\mathbf{V}}\| \leq \sqrt{2} \|\sin\Theta(\mathbf{V}, \tilde{\mathbf{V}})\|. \quad (59)$$

Since $\tilde{\mathbf{V}}$ is also the right singular matrix of $\hat{\mathbf{P}}$, using Wedin's lemma [Wed72] we know:

$$\|\sin\Theta(\mathbf{V}, \tilde{\mathbf{V}})\| \leq \frac{\|\mathbf{P} - \hat{\mathbf{P}}\|}{\sigma_r(\mathbf{P})}. \quad (60)$$

Combining above two inequalities and Eqn.(15) finishes the proof. \square

A.2 Proof of Theorem 1

Proof. We consider the KME $\mu_p(\cdot, \cdot) \in \mathcal{H} \times \tilde{\mathcal{H}}$ where $\mathcal{H} \times \tilde{\mathcal{H}}$ is the product RKHS, $K(x, y) = \Phi(x)^T \Phi(y)$ is the kernel of \mathcal{H} and $\tilde{K}(x, y) = \tilde{\Phi}(x)^T \tilde{\Phi}(y)$ is the kernel of $\tilde{\mathcal{H}}$. Suppose that $\{\Phi_i^\circ\}_{i=1}^M$ and $\{\tilde{\Phi}_i^\circ\}_{i=1}^{\tilde{M}}$ are respectively the orthonormal bases of \mathcal{H} and $\tilde{\mathcal{H}}$. $\{\Phi_i^\circ\}_{i=1}^M$ is an orthonormal basis for \mathcal{H} means

$$\langle \Phi_i^\circ, \Phi_j^\circ \rangle_{\mathcal{H}} = \begin{cases} 1, & i = j, \\ 0, & i \neq j. \end{cases} \quad (61)$$

Then there exist matrices $\mathbf{W} \in \mathbb{R}^{N \times M}$ and $\tilde{\mathbf{W}} \in \mathbb{R}^{N \times \tilde{M}}$ such that

$$\Phi(\cdot) = \mathbf{W} \Phi^\circ(\cdot), \quad \tilde{\Phi}(\cdot) = \tilde{\mathbf{W}} \tilde{\Phi}^\circ(\cdot). \quad (62)$$

Note that $\{\Phi_i^\circ\}_{i=1}^M$ is an orthonormal basis of \mathcal{H} implies that $K(x, y) = [\Phi^\circ(x)]^T [\Phi^\circ(y)]$, this is because $K(x, \cdot) \in \mathcal{H}$, so we can write it as:

$$K(x, \cdot) = \sum_{i=1}^M a_{x,i} \Phi_i^\circ(\cdot), \quad (63)$$

where $a_{x,i}$ is the coefficient that depends on x . By reproducing property and above identity:

$$\Phi_j^\circ(x) = \langle K(x, \cdot), \Phi_j^\circ(\cdot) \rangle_{\mathcal{H}} \quad (64)$$

$$= \sum_{i=1}^M a_{x,i} \langle \Phi_i^\circ, \Phi_j^\circ \rangle_{\mathcal{H}} \quad (65)$$

$$= a_{x,j}. \quad (66)$$

Plug into (63):

$$K(x, \cdot) = \sum_{i=1}^M a_{x,i} \Phi_i^\circ(\cdot) = \sum_{i=1}^M \Phi_i^\circ(x) \Phi_i^\circ(\cdot). \quad (67)$$

Note that $K(x, y) = [\Phi^\circ(x)]^T \Phi^\circ(y)$ and $K(x, y) = [\Phi(x)]^T \Phi(y) = [\Phi^\circ(x)]^T \mathbf{W}^T \mathbf{W} \Phi^\circ(y)$, therefore,

$$[\Phi^\circ(x)]^T \Phi^\circ(y) = [\Phi^\circ(x)]^T \mathbf{W}^T \mathbf{W} \Phi^\circ(y). \quad (68)$$

We can take $x_1, x_2, \dots, x_M \in \Omega$ such that

$$\mathbf{\Phi}^\circ = [\Phi^\circ(x_1), \Phi^\circ(x_2), \dots, \Phi^\circ(x_M)]$$

is a non-singular matrix. Then (68) implies

$$(\mathbf{\Phi}^\circ)^T \mathbf{\Phi}^\circ = (\mathbf{\Phi}^\circ)^T \mathbf{W}^T \mathbf{W} \mathbf{\Phi}^\circ,$$

therefore,

$$\mathbf{W}^T \mathbf{W} = \mathbf{I}_M. \quad (69)$$

Similar arguments imply

$$\tilde{\mathbf{W}}^T \tilde{\mathbf{W}} = \mathbf{I}_{\tilde{M}}. \quad (70)$$

If a matrix $\mathbf{M} \in \mathbb{R}^{N \times N}$ satisfies $\mathbf{M} = \mathbf{W} \mathbf{M}^\circ \tilde{\mathbf{W}}^T$ for some $\mathbf{M}^\circ \in \mathbb{R}^{M \times \tilde{M}}$, then

$$\|\mathbf{M}\|_F^2 = \text{Tr}(\mathbf{M}^T \mathbf{M}) = \text{Tr}((\mathbf{W} \mathbf{M}^\circ \tilde{\mathbf{W}}^T)^T (\mathbf{W} \mathbf{M}^\circ \tilde{\mathbf{W}}^T)) \quad (71)$$

$$= \text{Tr}((\mathbf{M}^\circ)^T (\mathbf{W}^T \mathbf{W}) \mathbf{M}^\circ (\tilde{\mathbf{W}}^T \tilde{\mathbf{W}})) \quad (72)$$

$$= \text{Tr}((\mathbf{M}^\circ)^T \mathbf{M}^\circ) \quad (73)$$

$$= \|\mathbf{M}^\circ\|_F^2. \quad (74)$$

Recall the inner product on $\mathcal{H} \times \tilde{\mathcal{H}}$ is given by the inner product on \mathcal{H} and $\tilde{\mathcal{H}}$: for any $f_1 \otimes g_1 \in \mathcal{H} \times \tilde{\mathcal{H}}$ and $f_2 \otimes g_2 \in \mathcal{H} \times \tilde{\mathcal{H}}$,

$$\langle f_1 \otimes g_1, f_2 \otimes g_2 \rangle_{\mathcal{H} \times \tilde{\mathcal{H}}} = \langle f_1, f_2 \rangle_{\mathcal{H}} \langle g_1, g_2 \rangle_{\tilde{\mathcal{H}}}.$$

It follows that

$$\left\| [\Phi(\cdot)]^T \mathbf{M} \tilde{\Phi}(\cdot) \right\|_{\mathcal{H} \times \tilde{\mathcal{H}}}^2 = \left\| [\Phi^\circ(\cdot)]^T \mathbf{W}^T \mathbf{M} \tilde{\mathbf{W}} \tilde{\Phi}^\circ(\cdot) \right\|_{\mathcal{H} \times \tilde{\mathcal{H}}}^2 = \left\| [\Phi^\circ(\cdot)]^T \mathbf{M}^\circ \tilde{\Phi}^\circ(\cdot) \right\|_{\mathcal{H} \times \tilde{\mathcal{H}}}^2 \quad (75)$$

$$= \left\langle \sum_{i=1}^M \sum_{j=1}^{\tilde{M}} \Phi_i^\circ(\cdot) \mathbf{M}_{ij}^\circ \tilde{\Phi}_j(\cdot), \sum_{k=1}^M \sum_{p=1}^{\tilde{M}} \Phi_k^\circ(\cdot) \mathbf{M}_{kp}^\circ \tilde{\Phi}_p(\cdot) \right\rangle_{\mathcal{H} \times \tilde{\mathcal{H}}} \quad (76)$$

$$= \sum_{i,k=1}^M \sum_{j,p=1}^{\tilde{M}} \mathbf{M}_{ij}^\circ \mathbf{M}_{kp}^\circ \langle \Phi_i^\circ, \Phi_k^\circ \rangle_{\mathcal{H}} \langle \tilde{\Phi}_j^\circ, \tilde{\Phi}_p^\circ \rangle_{\tilde{\mathcal{H}}} \quad (77)$$

$$= \sum_{i=1}^M \sum_{j=1}^{\tilde{M}} (\mathbf{M}_{ij}^\circ)^2 \quad (78)$$

$$= \|\mathbf{M}^\circ\|_F^2 = \|\mathbf{M}\|_F^2. \quad (79)$$

We can conclude that

$$\|\Phi(\cdot)^T \mathbf{M} \tilde{\Phi}(\cdot)\|_{\mathcal{H} \times \tilde{\mathcal{H}}} = \|\mathbf{M}\|_F. \quad (80)$$

The matrix \mathbf{P} in our paper satisfies

$$\mathbf{P} = \int_{\Omega \times \Omega} p(x, y) \Phi(x) [\tilde{\Phi}(y)]^T dx dy = \mathbf{W} \left(\int_{\Omega \times \Omega} p(x, y) \Phi^\circ(x) [\tilde{\Phi}^\circ(y)]^T dx dy \right) \tilde{\mathbf{W}}^T. \quad (81)$$

We also have

$$\hat{\mathbf{P}} = \frac{1}{n} \sum_{t=1}^n \Phi(X_t) [\tilde{\Phi}(X_{t+1})]^T = \mathbf{W} \left(\frac{1}{n} \sum_{t=1}^n \Phi^\circ(X_t) [\tilde{\Phi}^\circ(X_{t+1})]^T \right) \tilde{\mathbf{W}}^T. \quad (82)$$

Therefore, $\hat{\mathbf{U}} = \mathbf{W} \mathbf{\Gamma}$ for some $\mathbf{\Gamma} \in \mathbb{R}^{M \times N}$ and $\hat{\mathbf{V}} = \tilde{\mathbf{W}} \tilde{\mathbf{\Gamma}}$ for some $\tilde{\mathbf{\Gamma}} \in \mathbb{R}^{\tilde{M} \times N}$. It further implies

$$\tilde{\mathbf{P}} = \hat{\mathbf{U}} \hat{\mathbf{\Sigma}}_{[1 \dots r]} \hat{\mathbf{V}}^T = \mathbf{W} (\mathbf{\Gamma} \hat{\mathbf{\Sigma}}_{[1 \dots r]} \tilde{\mathbf{\Gamma}}^T) \tilde{\mathbf{W}}^T. \quad (83)$$

Then using (80) we know that:

$$\|\mu_P - \hat{\mu}_P\|_{\mathcal{H} \times \tilde{\mathcal{H}}} = \|\mathbf{P} - \tilde{\mathbf{P}}\|_F \leq \sqrt{2r} \|\mathbf{P} - \hat{\mathbf{P}}\|, \quad (84)$$

where the inequality follows the fact that \mathbf{P} and $\tilde{\mathbf{P}}$ are both of rank at most r hence $\mathbf{P} - \tilde{\mathbf{P}}$ has rank at most $2r$. According to Weyl's inequality [Wey12], $\|\hat{\mathbf{P}} - \tilde{\mathbf{P}}\| = \sigma_{r+1}(\hat{\mathbf{P}}) \leq \|\hat{\mathbf{P}} - \mathbf{P}\|$. It follows that

$$\|\mathbf{P} - \tilde{\mathbf{P}}\| \leq \|\mathbf{P} - \hat{\mathbf{P}}\| + \|\hat{\mathbf{P}} - \tilde{\mathbf{P}}\| \leq 2\|\hat{\mathbf{P}} - \mathbf{P}\|.$$

Using Eqn.(15) we finish the proof. \square

B Proof of Results in Section 4

B.1 Representation of $p(\cdot|\cdot)$

Lemma 10. Under Assumption 1-2, $p(\cdot|\cdot)$ has following representation:

$$p(y|x) = \Phi(x)^T \mathbf{C}^{-1} \mathbf{P} \tilde{\mathbf{C}}^{-1} \tilde{\Phi}(y). \quad (85)$$

where $\mathbf{P} := \int \pi(x) p(y|x) \Phi(x) \tilde{\Phi}(y)^T dx dy$, $\mathbf{C} := \text{diag}[\rho_1, \dots, \rho_N]$ and $\tilde{\mathbf{C}} := \text{diag}[\tilde{\rho}_1, \dots, \tilde{\rho}_N]$.

Proof. We know that $\Upsilon(\cdot) := \mathbf{C}^{-1/2} \Phi(\cdot)$ is a vector of orthonormal functions in $L^2(\pi)$, and $\tilde{\Upsilon}(\cdot) := \tilde{\mathbf{C}}^{-1/2} \tilde{\Phi}(\cdot)$ is a vector of orthonormal functions in L^2 . Then the coefficient matrix of $p(\cdot|\cdot)$ in expansion under $L^2(\pi) \times L^2$ inner product is given by:

$$\int \pi(x) p(y|x) \mathbf{C}^{-1/2} \Phi(x) \tilde{\Phi}(y)^T \tilde{\mathbf{C}}^{-1/2} dx dy = \mathbf{C}^{-1/2} \left(\int \pi(x) p(y|x) \Phi(x) \tilde{\Phi}(y)^T dx dy \right) \tilde{\mathbf{C}}^{-1/2} \quad (86)$$

$$= \mathbf{C}^{-1/2} \mathbf{P} \tilde{\mathbf{C}}^{-1/2}. \quad (87)$$

Then we have:

$$p(y|x) = \Upsilon(x)^T \mathbf{C}^{-1/2} \mathbf{P} \tilde{\mathbf{C}}^{-1/2} \tilde{\Upsilon}(y) \quad (88)$$

$$= \Phi(x)^T \mathbf{C}^{-1} \mathbf{P} \tilde{\mathbf{C}}^{-1} \tilde{\Phi}(y). \quad (89)$$

\square

B.2 Proof of Theorem 2

Proof. To simplify notation, denote $\mathbf{R} := \mathbf{C}^{-1/2} \mathbf{P} \tilde{\mathbf{C}}^{-1/2}$. Let $\mathbf{U}^{(\rho)} \Sigma_{[1 \dots r]}^{(\rho)} (\mathbf{V}^{(\rho)})^T = \mathbf{R}$ be the SVD of \mathbf{R} . Similarly we use $\hat{\mathbf{R}} := \mathbf{C}^{-1/2} \hat{\mathbf{P}} \tilde{\mathbf{C}}^{-1/2}$ with SVD $\hat{\mathbf{U}}^{(\rho)} \hat{\Sigma}_{[1 \dots r]}^{(\rho)} (\hat{\mathbf{V}}^{(\rho)})^T = \hat{\mathbf{R}}$. Let $\tilde{\mathbf{R}} := \hat{\mathbf{U}}^{(\rho)} \hat{\Sigma}_{[1 \dots r]}^{(\rho)} (\hat{\mathbf{V}}^{(\rho)})^T$ be the best rank r approximation of $\hat{\mathbf{R}}$. Use $\mathbb{O}_{r \times r}$ to denote set of all $r \times r$ orthogonal matrices, let $\mathbf{O} \in \mathbb{O}_{r \times r}$, using triangle inequality we have:

$$\begin{aligned} \|\Psi(x) - \Psi(z)\| &= \|\mathbf{O}\Psi(x) - \mathbf{O}\Psi(z)\| \\ &\leq \|\mathbf{O}\Psi(x) - \hat{\Psi}(x)\| + \|\hat{\Psi}(x) - \hat{\Psi}(z)\| + \|\mathbf{O}\Psi(z) - \hat{\Psi}(z)\|, \end{aligned} \quad (90)$$

this yields:

$$\widehat{dist}(x, z) - \widehat{dist}(x, z) = \|\Psi(x) - \Psi(z)\| - \|\hat{\Psi}(x) - \hat{\Psi}(z)\| \quad (91)$$

$$\leq \|\mathbf{O}\Psi(x) - \hat{\Psi}(x)\| + \|\mathbf{O}\Psi(z) - \hat{\Psi}(z)\|. \quad (92)$$

Similarly we can get:

$$\widehat{dist}(x, z) - dist(x, z) = \|\hat{\Psi}(x) - \hat{\Psi}(z)\| - \|\Psi(x) - \Psi(z)\| \quad (93)$$

$$\leq \|\mathbf{O}\Psi(x) - \hat{\Psi}(x)\| + \|\mathbf{O}\Psi(z) - \hat{\Psi}(z)\|. \quad (94)$$

Therefore, taking infimum over $\mathbf{O} \in \mathbb{O}_{r \times r}$ we have:

$$\left| dist(x, z) - \widehat{dist}(x, z) \right| \leq \inf_{\mathbf{O} \in \mathbb{O}_{r \times r}} \|\mathbf{O}\Psi(x) - \hat{\Psi}(x)\| + \|\mathbf{O}\Psi(z) - \hat{\Psi}(z)\| \quad (95)$$

$$\begin{aligned} &= \inf_{\mathbf{O} \in \mathbb{O}_{r \times r}} \|\Phi(x)^T \mathbf{C}^{-1/2} (\mathbf{U}^{(\rho)} \Sigma_{[1 \dots r]}^{(\rho)} \mathbf{O}^T - \hat{\mathbf{U}}^{(\rho)} \hat{\Sigma}_{[1 \dots r]}^{(\rho)})\| \\ &\quad + \|\Phi(z)^T \mathbf{C}^{-1/2} (\mathbf{U}^{(\rho)} \Sigma_{[1 \dots r]}^{(\rho)} \mathbf{O}^T - \hat{\mathbf{U}}^{(\rho)} \hat{\Sigma}_{[1 \dots r]}^{(\rho)})\| \end{aligned} \quad (96)$$

$$\leq \inf_{\mathbf{O} \in \mathbb{O}_{r \times r}} 2L_{max}^{1/2} \|\mathbf{U}^{(\rho)} \Sigma_{[1 \dots r]}^{(\rho)} \mathbf{O}^T - \hat{\mathbf{U}}^{(\rho)} \hat{\Sigma}_{[1 \dots r]}^{(\rho)}\| \quad (97)$$

$$= \inf_{\mathbf{O} \in \mathbb{O}_{r \times r}} 2L_{max}^{1/2} \|\mathbf{R} \mathbf{V}^{(\rho)} \mathbf{O}^T - \tilde{\mathbf{R}} \hat{\mathbf{V}}^{(\rho)}\| \quad (98)$$

$$= \inf_{\mathbf{O} \in \mathbb{O}_{r \times r}} 2L_{max}^{1/2} \|\mathbf{R} (\mathbf{V}^{(\rho)} \mathbf{O}^T - \hat{\mathbf{V}}^{(\rho)}) + (\mathbf{R} - \tilde{\mathbf{R}}) \hat{\mathbf{V}}^{(\rho)}\| \quad (99)$$

$$\leq \inf_{\mathbf{O} \in \mathbb{O}_{r \times r}} 2L_{max}^{1/2} \left(\|\mathbf{R}\| \cdot \|\mathbf{V}^{(\rho)} \mathbf{O}^T - \hat{\mathbf{V}}^{(\rho)}\| + \|\mathbf{R} - \tilde{\mathbf{R}}\| \cdot \|\hat{\mathbf{V}}^{(\rho)}\| \right) \quad (100)$$

$$= \inf_{\mathbf{O} \in \mathbb{O}_{r \times r}} 2L_{max}^{1/2} \left(\|\mathbf{R}\| \cdot \|\mathbf{V}^{(\rho)} \mathbf{O}^T - \hat{\mathbf{V}}^{(\rho)}\| + \|\mathbf{R} - \tilde{\mathbf{R}}\| \right) \quad (101)$$

$$\leq 2L_{max}^{1/2} (\|\mathbf{R}\| \sqrt{2} \|\sin \Theta(\mathbf{V}^{(\rho)}, \hat{\mathbf{V}}^{(\rho)})\| + \|\mathbf{R} - \tilde{\mathbf{R}}\|) \quad (102)$$

$$\leq 2L_{max}^{1/2} (\sqrt{2} \|\mathbf{R}\| \frac{\|\mathbf{R} - \tilde{\mathbf{R}}\|}{\sigma_r(\mathbf{R})} + \|\mathbf{R} - \tilde{\mathbf{R}}\|) \quad (103)$$

$$\leq 2L_{max}^{1/2} (1 + \sqrt{2} \kappa(\mathbf{R})) \|\mathbf{R} - \tilde{\mathbf{R}}\| \quad (104)$$

$$\leq 4L_{max}^{1/2} (1 + \sqrt{2} \kappa(\mathbf{R})) \|\mathbf{R} - \hat{\mathbf{R}}\| \quad (105)$$

$$= 4L_{max}^{1/2} (1 + \sqrt{2} \kappa(\mathbf{R})) \|\mathbf{C}^{-1/2} (\mathbf{P} - \hat{\mathbf{P}}) \tilde{\mathbf{C}}^{-1/2}\| \quad (106)$$

$$\leq 4 \sqrt{\frac{L_{max}}{\rho_N \tilde{\rho}_N}} \left[1 + \sqrt{2} \kappa(\mathbf{R}) \right] \|\mathbf{P} - \hat{\mathbf{P}}\|, \quad (107)$$

where from (104) to (105) we use Weyl's inequality [Wey12] and the fact that rank of $\tilde{\mathbf{R}}$ is r to get $\sigma_{r+1}(\tilde{\mathbf{R}}) \leq \|\mathbf{R} - \tilde{\mathbf{R}}\|$, therefore,

$$\|\mathbf{R} - \tilde{\mathbf{R}}\| \leq \|\mathbf{R} - \hat{\mathbf{R}}\| + \|\tilde{\mathbf{R}} - \hat{\mathbf{R}}\| = \|\mathbf{R} - \hat{\mathbf{R}}\| + \sigma_{r+1}(\hat{\mathbf{R}}) \leq 2\|\mathbf{R} - \hat{\mathbf{R}}\|. \quad (108)$$

Note that \mathbf{R} is the coefficient matrix of $p(y|x)$ in expansion with bases $\{\frac{\Phi_i(\cdot)}{\sqrt{\rho_i}}\}_{i=1}^N \times \{\frac{\tilde{\Phi}_i(\cdot)}{\sqrt{\tilde{\rho}_i}}\}_{i=1}^N$ using $L^2(\pi) \times L^2$ inner product, equivalently it is coefficient matrix of $\sqrt{\pi(x)} p(y|x)$ in expansion with bases $\{\frac{\Phi_i(\cdot) \sqrt{\pi(\cdot)}}{\sqrt{\rho_i}}\}_{i=1}^N \times \{\frac{\tilde{\Phi}_i(\cdot)}{\sqrt{\tilde{\rho}_i}}\}_{i=1}^N$ using $L^2 \times L^2$ inner product. By assumption 2, $\sqrt{\pi(x)} p(y|x)$ can be represented using $\{\frac{\Phi_i(\cdot) \sqrt{\pi(\cdot)}}{\sqrt{\rho_i}}\}_{i=1}^N \times \{\frac{\tilde{\Phi}_i(\cdot)}{\sqrt{\tilde{\rho}_i}}\}_{i=1}^N$, therefore we have $\kappa\left(\sqrt{\pi(x)} p(y|x)\right) = \kappa(\mathbf{R})$. We conclude proof using Eqn.(15). \square

B.3 Proof of Theorem 3

Proof. We show that $\|p(\cdot|x) - \hat{p}(\cdot|x)\|_{L^2(\pi) \times L^2} = \|\mathbf{R} - \tilde{\mathbf{R}}\|_F$. From Lemma 10 and definition of $\hat{p}(y|x)$ we have:

$$p(y|x) = \Phi(x)^T \mathbf{C}^{-1} \mathbf{P} \tilde{\mathbf{C}}^{-1} \tilde{\Phi}(y) = \Phi(x)^T \mathbf{C}^{-1/2} \mathbf{R} \tilde{\mathbf{C}}^{-1/2} \tilde{\Phi}(y), \quad (109)$$

$$\hat{p}(y|x) = \Phi(x)^T \mathbf{C}^{-1/2} \tilde{\mathbf{R}} \tilde{\mathbf{C}}^{-1/2} \tilde{\Phi}(y). \quad (110)$$

Then we have:

$$p(y|x) - \hat{p}(y|x) = \Phi(x)^T \mathbf{C}^{-1/2} (\mathbf{R} - \tilde{\mathbf{R}}) \tilde{\mathbf{C}}^{-1/2} \tilde{\Phi}(y). \quad (111)$$

Recall that $\Upsilon(\cdot) := \mathbf{C}^{-1/2} \Phi(\cdot)$ is a vector of orthonormal functions in $L^2(\pi)$ and $\tilde{\Upsilon}(\cdot) := \tilde{\mathbf{C}}^{-1/2} \tilde{\Phi}(\cdot)$ is a vector of orthonormal functions in L^2 . Then we have:

$$\|p(\cdot|x) - \hat{p}(\cdot|x)\|_{L^2(\pi) \times L^2} = \|\Phi(\cdot)^T \mathbf{C}^{-1/2} (\mathbf{R} - \tilde{\mathbf{R}}) \tilde{\mathbf{C}}^{-1/2} \tilde{\Phi}(\cdot)\| \quad (112)$$

$$= \|\Upsilon(\cdot) (\mathbf{R} - \tilde{\mathbf{R}}) \tilde{\Upsilon}(\cdot)\|_{L^2(\pi) \times L^2} \quad (113)$$

$$= \|\mathbf{R} - \tilde{\mathbf{R}}\|_F. \quad (114)$$

Combining (108) with (114) yields

$$\|p(\cdot|x) - \hat{p}(\cdot|x)\|_{L^2(\pi) \times L^2} = \|\mathbf{R} - \tilde{\mathbf{R}}\|_F \quad (115)$$

$$\leq \sqrt{r} \|\mathbf{R} - \tilde{\mathbf{R}}\| \quad (116)$$

$$\leq 2\sqrt{r} \|\mathbf{R} - \hat{\mathbf{R}}\| \quad (117)$$

$$= 2\sqrt{r} \|\mathbf{C}^{-1/2} (\mathbf{P} - \hat{\mathbf{P}}) \tilde{\mathbf{C}}^{-1/2}\| \quad (118)$$

$$\leq 2\sqrt{\frac{r}{\rho_N \hat{\rho}_N}} \|\mathbf{P} - \hat{\mathbf{P}}\|. \quad (119)$$

We conclude the proof upon using (15). \square

C Proof of Results in Section 5

C.1 Technical Lemmas

Lemma 11. Under Assumption 1-2, for each $q_i^*(\cdot)$, it can be written as:

$$q_i^*(\cdot) = \sum_{k=1}^r z_{ik} v_k(\cdot), \quad (120)$$

where $v_k(\cdot)$ are the right singular functions for $p(\cdot|x)$. Each $q_i^*(\cdot)$ is a probability density function.

Proof. $\{\Omega_i^*\}_{i=1}^m$ forms the best partition in terms of solving k-means problem. Then on each Ω_i^* , we must have $q_i^*(\cdot)$ solves the problem

$$\min_{q_i(\cdot) \in \mathcal{H}} \int_{\Omega_i^*} \pi(x) \|p(\cdot|x) - q_i(\cdot)\|_{L^2}^2 dx. \quad (121)$$

This is solved by

$$q_i^*(\cdot) = \frac{1}{\pi(\Omega_i^*)} \int_{\Omega_i^*} \pi(x) p(\cdot|x) dx. \quad (122)$$

To show $q_i^*(\cdot)$ is probability distribution, note that $q_i^*(y) \geq 0$ for all y because $p(y|x) \geq 0$ for all y and x . Furthermore, we have:

$$\int_{\Omega^*} q_i^*(y) dy = \frac{1}{\pi(\Omega_i^*)} \int_{\Omega} \int_{\Omega_i^*} \pi(x) p(y|x) dx dy \quad (123)$$

$$= \frac{1}{\pi(\Omega_i^*)} \int_{\Omega_i^*} \int_{\Omega} \pi(x) p(y|x) dy dx \quad (124)$$

$$= \frac{1}{\pi(\Omega_i^*)} \int_{\Omega_i^*} \pi(x) dx \quad (125)$$

$$= 1. \quad (126)$$

Without loss of generality, we assume that decomposition $p(y|x) = \sum_{i=1}^r \sigma_k u_k(x) v_k(x)$ in Assumption 1 is the SVD, i.e.,

$$\sigma_k = \Sigma_{k,k}^{(\rho)}, \quad u_k(\cdot) = (\mathbf{U}_{[:,k]}^{(\rho)})^T \mathbf{C}^{-1/2} \Phi(\cdot), \quad v_k(\cdot) = (\mathbf{V}_{[:,k]}^{(\rho)})^T \tilde{\mathbf{C}}^{-1/2} \tilde{\Phi}(\cdot).$$

To prove Eqn.(120), we plug in SVD of $p(y|x)$ into Eqn.(122):

$$q_i^*(\cdot) = \frac{1}{\pi(\Omega_i^*)} \int_{\Omega_i^*} \pi(x) p(\cdot|x) dx \quad (127)$$

$$= \sum_{k=1}^r \frac{\sigma_k}{\pi(\Omega_i^*)} \int_{\Omega_i^*} \pi(x) u_k(x) v_k(\cdot) dx. \quad (128)$$

Taking $z_{ik} := \frac{\sigma_k}{\pi(\Omega_i^*)} \int_{\Omega_i^*} \pi(x) u_k(x) dx$, we finish the proof. \square

Next lemma is key to prove Theorem 5. Before proving the lemma, we define a function $T(\cdot|x)$ that represents the perturbation of $p(\cdot|x)$ from its closest probability distribution $q_i^*(\cdot)$:

$$T(\cdot|x) = \sum_{i=1}^m \mathbb{1}_{\Omega_i^*}(x) \left(p(\cdot|x) - q_i^*(\cdot) \right). \quad (129)$$

By definition of Δ_2^2 we know that:

$$\|T(\cdot|x)\|_{L^2(\pi) \times L^2}^2 = \Delta_2^2. \quad (130)$$

Equivalently, one can rewrite the k-means problem in \mathbb{R}^r using the $\Psi(\cdot)$ coordinate as:

$$\min_{(\Omega_1, \dots, \Omega_m)} \min_{s_1, \dots, s_k \in \mathbb{R}^r} \sum_{i=1}^m \int_{\Omega_i} \pi(x) \|\Psi(x) - s_i\|_{l_2}^2 dx.$$

We showed in Lemma 6 that $s_i^* = [z_{i1}, \dots, z_{ir}]^T$, then we construct function $E(\cdot) : \Omega \rightarrow \mathbb{R}^r$ by:

$$E(x) = \sum_{i=1}^m \mathbb{1}_{\Omega_i^*}(x) (\Psi(x) - [z_{i1}, \dots, z_{ir}]^T). \quad (131)$$

It is easy to verify that

$$\Psi(x) = \mathbf{Z}\theta(x) + E(x), \quad (132)$$

where $\mathbf{Z} = [z_{ij}]_{r \times m}$ is given in Lemma 5, $\theta := [\mathbb{1}_{\Omega_1^*}, \dots, \mathbb{1}_{\Omega_m^*}]^T$, moreover, since $E(\cdot)$ is the counterpart of $T(\cdot|x)$ in \mathbb{R}^r , we have:

$$\|E(\cdot)\|_{L^2(\pi)}^2 = \Delta_2^2. \quad (133)$$

We further define following quantities which are useful for the statement of the lemma:

$$\delta_k^2 := \min_{l \neq k} \|q_l^* - q_k^*\|_{L^2}^2 = \min_{1 \neq k} \|\mathbf{Z}_{*l} - \mathbf{Z}_{*k}\|, \quad (134)$$

$$\bar{\Psi}(x) := \hat{\mathbf{Z}}\hat{\theta}(x) \quad \hat{\mathbf{Z}}_{*i} = \hat{s}_i, \quad \hat{\theta}(x) := [\mathbb{1}_{\hat{\Omega}_1^*}, \dots, \mathbb{1}_{\hat{\Omega}_m^*}]^T. \quad (135)$$

We use $\mathbb{O}_{r \times r}$ to denote the set of all $r \times r$ orthogonal matrices. For any $\mathbf{O} \in \mathbb{O}_{r \times r}$, we define:

$$S_k(\mathbf{O}\bar{\Psi}) := \{x \in \Omega_k^* : \|\mathbf{O}\bar{\Psi}(x) - \mathbf{Z}_{*k}\| \geq \delta_k/2\}. \quad (136)$$

For the ease of notation, we will use S_k instead of $S_k(\mathbf{O}\bar{\Psi})$. For a vector valued function $A(\cdot) : \Omega \rightarrow \mathbb{R}^r$, let its $L^2(\pi)$ norm to be $\|A(\cdot)\|_{L^2(\pi)} := \left(\int_{\Omega} \pi(x) \|A(x)\|_{\ell_2}^2 dx \right)^{1/2}$.

Lemma 12. *With quantities defined above, for any $\mathbf{O} \in \mathbb{O}_{r \times r}$ we have:*

$$\sum_{k=1}^m \pi(S_k) \delta_k^2 \leq 16 \left(\|\mathbf{O}\hat{\Psi}(\cdot) - \Psi(\cdot)\|_{L^2(\pi)} + \|E(\cdot)\|_{L^2(\pi)} \right)^2 \quad (137)$$

$$= 16 \left(\|\mathbf{U}^{(\rho)} \Sigma_{[1 \dots r]}^{(\rho)} \mathbf{O} - \hat{\mathbf{U}}^{(\rho)} \hat{\Sigma}_{[1 \dots r]}^{(\rho)}\|_F + \Delta_2 \right)^2. \quad (138)$$

In addition, if for any $1 \leq k \leq m$ we have:

$$\frac{16 \left(\|\mathbf{U}^{(\rho)} \Sigma_{[1 \dots r]}^{(\rho)} \mathbf{O} - \hat{\mathbf{U}}^{(\rho)} \hat{\Sigma}_{[1 \dots r]}^{(\rho)}\|_F + \Delta_2 \right)^2}{\delta_k^2} < \pi(\Omega_k^*). \quad (139)$$

Then every data point on $G := \cup_{k=1}^r (\Omega_k^* \setminus S_k)$ is correctly classified.

Proof. We follow the proof of Lemma 5.3 in [LR⁺15]. By definition of S_k , we have:

$$\sum_{k=1}^m \pi(S_k) \delta_k^2 \leq 4 \sum_{k=1}^m \int_{S_k} \pi(x) \|\mathbf{O}\bar{\Psi}(x) - \mathbf{Z}_{*k}\|^2 dx \quad (140)$$

$$\leq 4 \int_{\Omega} \pi(x) \|\mathbf{O}\bar{\Psi}(x) - \mathbf{Z}\theta(x)\|^2 dx \quad (141)$$

$$= 4 \|\mathbf{O}\bar{\Psi}(\cdot) - \mathbf{Z}\theta(\cdot)\|_{L^2(\pi)}^2. \quad (142)$$

To bound $\|\mathbf{O}\bar{\Psi}(\cdot) - \mathbf{Z}\theta(\cdot)\|_{L^2(\pi)}$:

$$\begin{aligned} & \|\mathbf{O}\bar{\Psi}(\cdot) - \mathbf{Z}\theta(\cdot)\|_{L^2(\pi)} \\ & \leq \|\mathbf{O}\bar{\Psi}(\cdot) - \mathbf{O}\hat{\Psi}(\cdot)\|_{L^2(\pi)} + \|\mathbf{O}\hat{\Psi}(\cdot) - \Psi(\cdot)\|_{L^2(\pi)} + \|\Psi(\cdot) - \mathbf{Z}\theta(\cdot)\|_{L^2(\pi)} \end{aligned} \quad (143)$$

$$= \|\bar{\Psi}(\cdot) - \hat{\Psi}(\cdot)\|_{L^2(\pi)} + \|\mathbf{O}\hat{\Psi}(\cdot) - \Psi(\cdot)\|_{L^2(\pi)} + \|E(\cdot)\|_{L^2(\pi)}, \quad (144)$$

where we use the fact that $\Psi(x) = \mathbf{Z}\theta(x) + E(x)$. Because $\bar{\Psi}(x) = \hat{\mathbf{Z}}\hat{\theta}(\cdot)$ solves the empirical k-means problem,

$$\begin{aligned} \|\bar{\Psi}(\cdot) - \hat{\Psi}(\cdot)\|_{L^2(\pi)} & \leq \|\mathbf{O}^T \mathbf{Z}\theta(\cdot) - \hat{\Psi}(\cdot)\|_{L^2(\pi)} = \|\mathbf{Z}\theta(\cdot) - \mathbf{O}\hat{\Psi}(\cdot)\|_{L^2(\pi)} \\ & \leq \|\mathbf{Z}\theta(x) - \Psi(\cdot)\|_{L^2(\pi)} + \|\mathbf{O}\hat{\Psi}(\cdot) - \Psi(\cdot)\|_{L^2(\pi)} \\ & = \|E(\cdot)\|_{L^2(\pi)} + \|\mathbf{O}\hat{\Psi}(\cdot) - \Psi(\cdot)\|_{L^2(\pi)}. \end{aligned} \quad (145)$$

Plugging (145) into (144) gives

$$\|\mathbf{O}\bar{\Psi}(\cdot) - \mathbf{Z}\theta(\cdot)\|_{L^2(\pi)} \leq 2\|\mathbf{O}\hat{\Psi}(x) - \Psi(x)\|_{L^2(\pi)} + 2\|E(\cdot)\|_{L^2(\pi)}. \quad (146)$$

It follows from Eqn.(142) that

$$\sum_{k=1}^m \pi(S_k) \delta_k^2 \leq 16 \left(\|\mathbf{O}\hat{\Psi}(x) - \Psi(x)\|_{L^2(\pi)} + \|E(\cdot)\|_{L^2(\pi)} \right)^2 \quad (147)$$

$$= 16 \left(\|\mathbf{O}\hat{\Psi}(x) - \Psi(x)\|_{L^2(\pi)} + \Delta_2 \right)^2. \quad (148)$$

We then show: $\|\mathbf{O}\hat{\Psi}(x) - \Psi(x)\|_{L^2(\pi)}^2 = \|\mathbf{U}^{(\rho)} \Sigma_{[1 \dots r]}^{(\rho)} \mathbf{O} - \hat{\mathbf{U}}^{(\rho)} \hat{\Sigma}_{[1 \dots r]}^{(\rho)}\|_F^2$:

$$\|\mathbf{O}\hat{\Psi}(x) - \Psi(x)\|_{L^2(\pi)}^2 = \|\hat{\Psi}(x) - \mathbf{O}^T \Psi(x)\|_{L^2(\pi)}^2 \quad (149)$$

$$\begin{aligned} & = \int_{\Omega} \pi(x) \Phi(x)^T \mathbf{C}^{-1/2} (\mathbf{U}^{(\rho)} \Sigma_{[1 \dots r]}^{(\rho)} \mathbf{O} - \hat{\mathbf{U}}^{(\rho)} \hat{\Sigma}_{[1 \dots r]}^{(\rho)}) \\ & \quad \cdot (\mathbf{U}^{(\rho)} \Sigma_{[1 \dots r]}^{(\rho)} \mathbf{O} - \hat{\mathbf{U}}^{(\rho)} \hat{\Sigma}_{[1 \dots r]}^{(\rho)})^T \mathbf{C}^{-1/2} \Phi(x) dy \end{aligned} \quad (150)$$

$$= \text{Tr} \left((\mathbf{U}^{(\rho)} \Sigma_{[1 \dots r]}^{(\rho)} \mathbf{O} - \hat{\mathbf{U}}^{(\rho)} \hat{\Sigma}_{[1 \dots r]}^{(\rho)}) (\mathbf{U}^{(\rho)} \Sigma_{[1 \dots r]}^{(\rho)} \mathbf{O} - \hat{\mathbf{U}}^{(\rho)} \hat{\Sigma}_{[1 \dots r]}^{(\rho)})^T \right) \quad (151)$$

$$= \|\mathbf{U}^{(\rho)} \Sigma_{[1 \dots r]}^{(\rho)} \mathbf{O} - \hat{\mathbf{U}}^{(\rho)} \hat{\Sigma}_{[1 \dots r]}^{(\rho)}\|_F^2. \quad (152)$$

Plug this back into Eqn.(147)

$$\sum_{k=1}^m \pi(S_k) \delta_k^2 \leq 16 \left(\|\mathbf{U}^{(\rho)} \Sigma_{[1 \dots r]}^{(\rho)} \mathbf{O} - \hat{\mathbf{U}}^{(\rho)} \hat{\Sigma}_{[1 \dots r]}^{(\rho)}\|_F + \Delta_2 \right)^2. \quad (153)$$

which finishes the proof of Eqn.(137).

We then prove if condition (139) holds, then every data point on $G := \cup_{k=1}^r (\Omega_k^* \setminus S_k)$ is correctly classified. From Eqn.(137):

$$\pi(S_k) \delta_k^2 \leq \sum_{k=1}^m \pi(S_k) \delta_k^2 \leq 16 \left(\|\mathbf{U}^{(\rho)} \Sigma_{[1 \dots r]}^{(\rho)} \mathbf{O} - \hat{\mathbf{U}}^{(\rho)} \hat{\Sigma}_{[1 \dots r]}^{(\rho)}\|_F + \Delta_2 \right)^2. \quad (154)$$

If condition (139) holds, dividing δ_k^2 on both sides of Eqn.(154) gives:

$$\pi(S_k) \leq \frac{16 \left(\|\mathbf{O}\hat{\Psi}(x) - \Psi(x)\|_{L^2(\pi)} + \Delta_2 \right)^2}{\delta_k^2} < \pi(\Omega_k^*). \quad (155)$$

From this we know $T_k := \Omega_k^* \setminus S_k \neq \emptyset$ for all k . We then prove data on T_k are correctly classified for any k . If $x \in T_k, y \in T_l$ for $k \neq l$, we must have $\bar{\Psi}(x) \neq \bar{\Psi}(y)$, otherwise we have

$$\max(\delta_k, \delta_l) \leq \|\mathbf{Z}_{*k} - \mathbf{Z}_{*l}\|_{l_2} \leq \|\mathbf{Z}_{*k} - \mathbf{O}\bar{\Psi}(x)\| + \|\mathbf{Z}_{*l} - \mathbf{O}\bar{\Psi}(y)\| < \delta_k/2 + \delta_l/2$$

which is impossible. On the other hand, of $x, y \in T_k$ for some k , then we must have $\bar{\Psi}(x) = \bar{\Psi}(y)$, otherwise $\bar{\Psi}(x)$ will take more than m values which is impossible due to its definition in Eqn.(135). \square

C.2 Proof of Theorem 4

Proof. For ease of notation we omit the perturbation σ . Let $\mathbb{O}_{r \times r}$ be the set of all $r \times r$ orthogonal matrices. Let $\mathbf{O} \in \mathbb{O}_{r \times r}$ be an $r \times r$ orthogonal matrix that will be specified later. Denote $\mathbf{R} = \mathbf{U}^{(\rho)} \boldsymbol{\Sigma}_{[1 \dots r]}^{(\rho)} (\mathbf{V}^{(\rho)})^T = \mathbf{C}^{-1/2} \mathbf{P} \tilde{\mathbf{C}}^{-1/2}$ and $\tilde{\mathbf{R}} = \hat{\mathbf{U}}^{(\rho)} \hat{\boldsymbol{\Sigma}}_{[1 \dots r]}^{(\rho)} (\hat{\mathbf{V}}^{(\rho)})^T$. From Eqn.(138) we have:

$$\sum_{k=1}^m \pi(S_k) \delta_k^2 \leq 16 \left(\|\mathbf{U}^{(\rho)} \boldsymbol{\Sigma}_{[1 \dots r]}^{(\rho)} \mathbf{O} - \hat{\mathbf{U}}^{(\rho)} \hat{\boldsymbol{\Sigma}}_{[1 \dots r]}^{(\rho)}\|_F + \Delta_2 \right)^2 \quad (156)$$

$$= 16 \left(\|\mathbf{R} \mathbf{V}^{(\rho)} \mathbf{O} - \tilde{\mathbf{R}} \hat{\mathbf{V}}^{(\rho)}\|_F + \Delta_2 \right)^2. \quad (157)$$

To bound $\|\mathbf{R} \mathbf{V}^{(\rho)} \mathbf{O} - \tilde{\mathbf{R}} \hat{\mathbf{V}}^{(\rho)}\|_F$:

$$\|\mathbf{R} \mathbf{V}^{(\rho)} \mathbf{O} - \tilde{\mathbf{R}} \hat{\mathbf{V}}^{(\rho)}\|_F = \|\mathbf{R} (\mathbf{V}^{(\rho)} \mathbf{O} - \hat{\mathbf{V}}^{(\rho)}) + (\mathbf{R} - \tilde{\mathbf{R}}) \hat{\mathbf{V}}^{(\rho)}\|_F \quad (158)$$

$$\leq \|\mathbf{R}\| \cdot \|\mathbf{V}^{(\rho)} \mathbf{O} - \hat{\mathbf{V}}^{(\rho)}\|_F + \|\mathbf{R} - \tilde{\mathbf{R}}\| \cdot \|\hat{\mathbf{V}}^{(\rho)}\|_F \quad (159)$$

$$= \|\mathbf{R}\| \cdot \|\mathbf{V}^{(\rho)} \mathbf{O} - \hat{\mathbf{V}}^{(\rho)}\|_F + \sqrt{r} \|\mathbf{R} - \tilde{\mathbf{R}}\|, \quad (160)$$

where on the last equality we use the fact that $\hat{\mathbf{V}}^{(\rho)}$ is orthogonal hence $\|\hat{\mathbf{V}}^{(\rho)}\|_F = \sqrt{r}$. We know that there exists some $\mathbf{O} \in \mathbb{O}_{r \times r}$ such that

$$\|\mathbf{V}^{(\rho)} \mathbf{O} - \hat{\mathbf{V}}^{(\rho)}\|_F \leq \sqrt{2} \|\sin \Theta(\mathbf{V}^{(\rho)}, \hat{\mathbf{V}}^{(\rho)})\|_F \leq \sqrt{2r} \|\sin \Theta(\mathbf{V}^{(\rho)}, \hat{\mathbf{V}}^{(\rho)})\|. \quad (161)$$

By Wedin's lemma and the fact that \mathbf{R} and $\tilde{\mathbf{R}}$ have rank r we know that

$$\|\mathbf{V}^{(\rho)} \mathbf{O} - \hat{\mathbf{V}}^{(\rho)}\|_F \leq \frac{\sqrt{2r} \|\mathbf{R} - \tilde{\mathbf{R}}\|}{\sigma_r(\mathbf{R})}. \quad (162)$$

Plug this back into Eqn.(160) we have:

$$\|\mathbf{R} \mathbf{V}^{(\rho)} \mathbf{O} - \tilde{\mathbf{R}} \hat{\mathbf{V}}^{(\rho)}\|_F \leq (\sqrt{r} + \frac{\sqrt{2r} \|\mathbf{R}\|}{\sigma_r(\mathbf{R})}) \|\mathbf{R} - \tilde{\mathbf{R}}\| \quad (163)$$

$$\leq 2\sqrt{2r} \kappa(\mathbf{R}) \|\mathbf{R} - \tilde{\mathbf{R}}\| \quad (164)$$

$$\leq 4\sqrt{2r} \kappa(\mathbf{R}) \|\mathbf{R} - \tilde{\mathbf{R}}\| \quad (165)$$

$$\leq 4\sqrt{\frac{2r}{\rho_N \tilde{\rho}_N}} \kappa(\mathbf{R}) \|\mathbf{P} - \hat{\mathbf{P}}\| \quad (166)$$

$$= 4\sqrt{\frac{2r}{\rho_N \tilde{\rho}_N}} \kappa \|\mathbf{P} - \hat{\mathbf{P}}\|, \quad (167)$$

where in the last equality we use the fact that $\kappa(\mathbf{R}) = \kappa \left(\sqrt{\pi(x)p(y|x)} \right)$ which we proved in the proof of Theorem 2.

According to Lemma 8, there exists a constant $c > 0$ such that if

$$n \geq c \cdot \frac{\kappa^2 r \bar{\lambda} t_{mix} \log(2t_{mix} N / \delta)}{\rho_N \tilde{\rho}_N} \cdot \max \left\{ \frac{1}{(\Delta_1/4 - \Delta_2)^2}, \frac{2}{\epsilon \Delta_1^2}, \frac{4\Delta_2^2}{\epsilon^2 \Delta_1^4} \right\}, \quad (168)$$

then with probability at least $1 - \delta$,

$$\|\hat{\mathbf{P}} - \mathbf{P}\| \leq \frac{1}{4\kappa(\mathbf{R})} \sqrt{\frac{\rho_N \tilde{\rho}_N}{2r}} \min \left\{ \Delta_1/4 - \Delta_2, \sqrt{\epsilon/2} \Delta_1, \frac{\epsilon \Delta_1^2}{2\Delta_2} \right\}. \quad (169)$$

Under condition (169), $16 \left(\|\mathbf{R} \mathbf{V}^{(\rho)} \mathbf{O} - \tilde{\mathbf{R}} \hat{\mathbf{V}}^{(\rho)}\|_F + \Delta_2 \right)^2 < \Delta_1^2$, which ensures (139) is true hence we can use Lemma 12. We also have $\|\mathbf{R} \mathbf{V}^{(\rho)} \mathbf{O} - \tilde{\mathbf{R}} \hat{\mathbf{V}}^{(\rho)}\|_F^2 \leq \epsilon \Delta_1^2/2$ and $\|\mathbf{R} \mathbf{V}^{(\rho)} \mathbf{O} - \tilde{\mathbf{R}} \hat{\mathbf{V}}^{(\rho)}\|_F \Delta_2 \leq \epsilon \Delta_1^2/2$. These

two inequalities together imply

$$16 \left(\|\mathbf{R}\mathbf{V}^{(\rho)}\mathbf{O} - \hat{\mathbf{R}}\hat{\mathbf{V}}^{(\rho)}\|_F + \Delta_2 \right)^2 \quad (170)$$

$$= 16 \left(\|\mathbf{R}\mathbf{V}^{(\rho)}\mathbf{O} - \hat{\mathbf{R}}\hat{\mathbf{V}}^{(\rho)}\|_F^2 + 2\|\mathbf{R}\mathbf{V}^{(\rho)}\mathbf{O} - \hat{\mathbf{R}}\hat{\mathbf{V}}^{(\rho)}\|_F \Delta_2 + \Delta_2^2 \right) \quad (171)$$

$$\leq \epsilon \Delta_1^2 + 16\Delta_2^2. \quad (172)$$

We can now derive an upper bound for the misclassification rate M :

$$M(\hat{\Omega}_1^*, \dots, \hat{\Omega}_m^*) \leq \sum_{k=1}^m \frac{\pi(S_k)}{\pi(\Omega_k^*)} \quad (173)$$

$$\leq \sum_{k=1}^m \frac{\pi(S_k) \delta_k^2}{\Delta_1^2} \quad (174)$$

$$\leq \frac{16 \left(\|\mathbf{R}\mathbf{V}^{(\rho)}\mathbf{O} - \hat{\mathbf{R}}\hat{\mathbf{V}}^{(\rho)}\|_F + \Delta_2 \right)^2}{\Delta_1^2} \quad (175)$$

$$\leq \epsilon + \frac{16\Delta_2^2}{\Delta_1^2}. \quad (176)$$

□

D Experiment with DQN

The game of Demon Attack is simulated in the Arcade Learning Environment ([BNVB13]), which provides an interface to hundreds of Atari 2600 games and serves an important testbed for deep reinforcement learning algorithms. We closely follow the experimental setting, network structure and training method used by [MKS⁺15]. In this environment, each game frame o_t is a $210 \times 160 \times 3$ image. In each interactive step the agent takes in the last 16 frames and preprocesses them to be the input state $s_t = \phi(\{o_{t-i}\}_{i=0}^{15})$. The state s_t is an $84 \times 84 \times 4$ rescaled, grey-scale image, and is the input to the neural network $Q(s_t, \cdot; \theta)$. The first convolution layer in the network has 32 filters of size 8 stride 4, the second layer has 64 layers of size 4 stride 2, the final convolution layer has 64 filters of size 3 stride 1, and is followed by a fully-connected hidden layer of 512 units. The output is another fully-connected layer with six units that correspond to the six action values $\{Q(s_t, a_i; \theta)\}_{i=1}^6$. The agent selects an action based on these state-action values, repeats the selected action four times, observes four subsequent frames $\{o_{t+i}\}_{i=1}^4$ and receives an accumulated reward r_t .

The agent in the DQN algorithm "learns" through a novel variant of Q-learning that employs the techniques of target net (θ^-) and experience replay (D) ([MKS⁺15]), and conducts gradient descent to the following loss function at each iteration:

$$\mathcal{L}(\theta) = \mathbf{E}_{s,a,r,s' \sim U(D)} \left[\left(r + \gamma \max_{a'} Q(s', a'; \theta^-) - Q(s, a; \theta) \right)^2 \right].$$

While our training regime and hyper-parameters are almost the same as those of [MKS⁺15], we use Adam optimizer ([KB15]) with a decaying learning rate, and a smaller replay buffer of size 500k frames. Training is done over 2.5 million steps, i.e., 10 million game frames. The Q-network is stored and evaluated every 500k steps. The best policy among these evaluations attains a 150-200% human-level performance (which was reported in [MKS⁺15]), and is later used as our sampling policy.

The raw input to the state embedding algorithm is a time series of length 47936 and dimension 512, comprising 130 trajectories generated by the fully-connected hidden layer in DQN when it is running the sampling policy. The embeddings are obtained through the same process as in Experiment 6.1 with a Gaussian kernel and 200 random Fourier features. The rank r is set to be 3, and the time interval τ corresponds to 12 game frames, i.e., 0.36 second in real time. Both the raw data and the embeddings are projected onto 2D planes by t-SNE with a perplexity of 40.